Inter-subunit Crosstalk via PDZ Synergistically Governs Allosteric Activation of Proapoptotic HtrA2

Aasna L. Parui, [1, 2] Vandana Mishra, [3] Shubhankar Dutta, [1] Prasenjit Bhaumik, [3] Kakoli Bose [1, 2,*]

[1]Advanced Centre for Treatment, Research and Education in Cancer (ACTREC), Tata Memorial Centre, Kharghar, Navi Mumbai – 410210, India.

[2]Homi Bhabha National Institute, BARC Training School Complex, Anushaktinagar, Mumbai – 400094, India.

[3]Department of Biosciences and Bioengineering, Indian Institute of Technology Bombay, Powai, Mumbai – 400076, India.

*Corresponding author

Correspondence to: Dr. Kakoli Bose, Integrated Biophysics and Structural Biology Lab, Advanced Centre for Treatment, Research and Education in Cancer (ACTREC), Tata Memorial Centre, Navi Mumbai –410210, Maharashtra, India.

Email: kbose@actrec.gov.in

RUNNING TITLE: *Trans*-mediated Allostery in HtrA2

ABSTRACT:

Mitochondrial serine protease – High temperature requirement A2 (HtrA2), is associated with various diseases including neurodegenerative disorders and cancer. Despite availability of structural details, the reports on HtrA2's mechanistic regulation that varies with the type of activation signals still remain non-concordant. To expound the role of regulatory PDZ domains in promoting synergistic coordination between HtrA2 subunits, we generated heterotrimeric HtrA2 variants comprising different numbers of PDZs and/or active-site mutations. Sequential deletion of PDZs from the trimeric ensemble significantly affected its residual activity in a way that proffered a hypothesis advocating *intermolecular* allosteric crosstalk via PDZ domains in trimeric HtrA2. Furthermore, structural and computational snapshots affirmed the role of PDZs in secondary structural element formation and coordinated reorganization of the N-terminal region and regulatory loops. Therefore, apart from providing cues for devising structure-guided therapeutic strategies, this study establishes a working model of complex allosteric regulation through a multifaceted *trans*-mediated cooperatively-shared energy landscape.

KEYWORDS: allostery/ensemble/intermolecular crosstalk/PDZ/*trans*-mediated activation

INTRODUCTION:

Cells respond to different environmental cues by channelizing distinct metabolic and/or signal transduction pathways, often controlled by allosteric enzymes with explicit biological functions. For highly regulated cellular scenarios, these allosteric enzymes are generally large multidomain protein ensembles that exhibit their regulatory roles through unique conformational adaptations. These modulations include minimal structural perturbations through subtle loop movements near the active-site and/or larger transitions involving reorientation of a domain with respect to another upon ligand binding at the allosteric pocket, leading to either active-site rearrangement or enhanced substrate catalysis (Ma et al, 2011; Traut, 2014). Interestingly, the second situation, where the individual globular domains confer a distinct spatial scaffold to the overall structural architecture, often correlates with a specific cellular function of the protein. Furthermore, these conserved regulatory domains have been evolutionarily tuned toward rewiring themselves to perform distinct functions in several unrelated proteins, which they achieve by accommodating themselves to global structural plasticity in diverse macromolecular milieu (Bagowski et al, 2010; Basu et al, 2009).

PDZ (Postsynaptic density-95/Discs large/Zonula occludens-1) domains are modular protein-protein interaction moieties that are found in many macromolecular protein ensembles, and are specialized for classically binding to C-terminal peptide motifs of various other proteins (Hung & Sheng, 2002; Kim & Sheng, 2004; Lee & Zheng, 2010). These structural scaffolds possess multiple ligand-binding sites, which contribute toward their unparallel conformational plasticity; thus, helping in relay of modulatory signals from a distal binding region to the functional site. Human HtrA2 (High temperature requirement protease A2) is a PDZ-bearing mitochondrial proapoptotic serine protease that is associated with different forms of pathogenesis including

arthritis, neurodegenerative disorders such as Parkinson's and Alzheimer's disease as well as cancer, and hence is an important therapeutic target (Joanna et al, 2013; Singh et al, 2011). It belongs to a large family of multi-domain serine proteases (S1, chymotrypsin family) with unique structural organization that is conserved from prokaryotes to humans (Clausen et al, 2011). All HtrA members reveal a common evolutionarily conserved higher-order architecture spanning from a trimer to a 24-mer oligomeric ensemble, with each subunit having either one or two PDZ domains. Despite these diversities, HtrAs share an overall conserved polypeptide fold with an active-site comprising a catalytic triad, an oxyanion hole and a substrate specificity pocket. However, prevalence of low sequence identity as well as ligand-induced subtle conformational variations provide the basis for their specificity and functional diversity. Through their distinct structural signatures, HtrAs regulate critical biological functions such as apoptosis, cell growth, protein quality control, and metabolism of amyloid precursor proteins. For example, while the bacterial homolog DegP has a temperature-dependent dual chaperone-protease activity, DegS is known to be a tightly regulated stress-responsive sensory protease. Similarly, this diverseness is also observed in the four human HtrAs (HtrA1-4) identified till date, where HtrA1, HtrA3 and HtrA4 are known to be associated with degeneration of extracellular matrix components, tumor suppressor activity and pre-eclampsia respectively (Singh et al, 2011; Vierkotten et al, 2011). One of the unique features that differentiates HtrA2 from rest of the family members is removal of transmembrane anchor and localization signal (133 residues) from the N-terminal region upon receiving an apoptotic signal. This cleavage not only translocates mature HtrA2 to the cytoplasm for execution of its proapoptotic activities, but also exposes a tetrapeptide motif (AVPS) at the N-terminal end for specific recognition and cleavage of inhibitor of apoptosis proteins (IAPs), thus promoting cell death through a binary mode of

activation (Yang et al, 2003). Apart from mediating caspase-dependent apoptosis by deactivating anti-apoptotic proteins such as XIAPs (X-Linked Inhibitor of Apoptosis Protein) (Suzuki et al, 2001a), its unique structural organization and domain plasticity have also enabled HtrA2 to promote the non-classical caspase-independent apoptotic pathways (Suzuki et al, 2001b) via its intricate serine protease activity. However, the complex mechanism through which it promotes initiation of apoptotic cascades or regulates protein quality control still remains elusive.

With respect to domain organization, mature HtrA2 comprises three important regions: a short N-terminal region that contains AVPS motif and part of the trimerization motif (residues Y147 and F149), a serine protease domain (SPD) harboring the catalytic triad (H198, D228, and S306) that is buried 25 Å into the central cavity of the pyramidal ensemble, and a single C-terminal PDZ domain gating the base of the trimeric assembly (Li et al, 2002). Although being evolutionarily non-conserved, a flexible linker at the PDZ-protease interface is implicated in assisting coordinated domain movement upon activation. A mechanistic model based on the first high resolution crystal structure of the catalytically inactive (S306A) apo-HtrA2 stated that PDZs, which otherwise stereochemically shield the proteolytically competent active-site pocket of the same monomer in the basal state, releases this inhibitory effect only upon ligand binding (Li et al, 2002). However, subsequent reports demonstrated a significant decrease in the protease activity of a PDZ-lacking variant (Bejugam et al, 2013; Chaganti et al, 2013). HtrA2 is known to be activated either upon ligand binding at a distal allosteric site (Gieldon et al, 2016; Martins et al, 2003) or by increase in temperature (Spiess et al, 1999; Zurawa-Janicka et al, 2013); these mechanisms are proposed to lead to displacement of the PDZ domain from the proximity of the active-site. This type of allosteric mechanism has also been observed in the bacterial counterpart DegS (Sohn et al, 2010), which exhibits significant sequence homology and an overall structural

similarity with HtrA2. However, unlike the basal state of HtrA2, the catalytic site of DegS has been found to be constantly exposed (Sohn et al, 2010), and its activity is governed by a more dominant *cis* PDZ-protease interaction induced upon binding of OMP (Outer Membrane Protein) peptides (Mauldin & Sauer, 2013). Besides, the activation of human counterpart HtrA1 has been found to be on the basis of conformational selection mode that regulates the functioning in a PDZ-independent manner (Cabrera et al, 2017). On the contrary, a dual regulatory switch conferred through the binding of allosteric ligands to the PDZs or other regions of the protein was found to be responsible for bringing about coordinated structural reorganizations at the distal regulatory loops essential for HtrA2 activation (Singh et al, 2014). Based on *in silico* and biophysical studies, many reports further hypothesized the involvement of intermolecular PDZ-protease crosstalk and conformational plasticity in the allosteric activation of HtrA2 (Chaganti et al, 2013; Gieldon et al, 2016; Martins et al, 2003; Spiess et al, 1999; Zurawa-Janicka et al, 2013). Although currently there are multiple crystallographic reports (Gieldon et al, 2016; Li et al, 2002; Merski et al, 2017b) of the apo-enzyme available with intact catalytic triad, these structural studies fail to elucidate the intricate conformational dynamics occurring in real-time with respect to different modes of enzyme activation viz. substrate binding or temperature.

Evolutionarily, PDZs are known to be greatly involved in determining the active and/or inactive state of HtrA oligomers. Apart from the unique N-terminal mediated regulation (Singh et al, 2014), the transition from the apo-form to the proteolytically active state of HtrA2 seems to be strictly governed by PDZs, owing to its highly specific interaction with numerous C-terminal binding partners such as cytoskeletal proteins and other apoptosis-related molecules. Although the available structural information signifies involvement of the regulatory loops in HtrA2 activation, what determines the specificity of PDZ domains toward a large repertoire of

substrates and how do these PDZs specifically relay the allosteric information to the three available catalytic protease domains are the questions yet remain to be answered. The basic requirement of HtrA family of proteases to exist as large oligomeric ensembles, despite having all the functional elements present in a single subunit, is quite astonishingly profound. The aim of this study is to recognize the importance of each subunit in attributing towards the dynamic energy landscape within the ensemble and to identify how PDZ domains from each subunit, besides allosterically regulating HtrA2 function help the trimer to attain an active functional state upon stimulation through different activation modes. To achieve this, we generated different heterotrimeric variants of HtrA2 that lack one or two PDZ domains and performed comprehensive enzyme kinetic analyses with a C-terminal binding partner. With the help of active-site chemical profiling (Liu et al, 1999) using the fully active heterotrimers and/or heterotrimers having specific protease domains inactivated, we established that binding of substrate to a single PDZ domain not only significantly affects the proteolytic activity of neighboring subunits, rather than the same attached subunit, but also compensates for the loss of active-sites within the ensemble. In case of both substrate- and temperature-based activations, we demonstrate an intricate predominant interdomain networking between the protease and PDZ domains (*trans* PDZ-protease crosstalk) that leads to subtle reorganization of the active-site loops and formation of a protease-substrate complex that is tuned for efficient catalysis. The networking is responsible for maintaining the overall proteolytic activities of each HtrA2 subunit via cooperatively-coupled energy dynamism within the trimeric pyramidal ensemble. Besides maintaining the oligomeric architecture and substrate specificity, this study emphasizes the importance of the evolutionarily conserved PDZ domain in determining the active functional state of the HtrA2 trimer that is catalytically more competent under a specific cellular scenario

and is also energetically most favorable. The concept encompassing such functionally important events, which can be transmitted long-range to affect the affinity or catalytic efficiency of a distant active-site, poses a challenge and necessity to identify the communication pathway underlying the functional effects of such larger macromolecular assemblies.

RESULTS:

Generation of heterotrimeric HtrA2 variants with different number of PDZ domains

For understanding the specific function of PDZ domains in propagating allosteric communication, we generated heterotrimeric variants of HtrA2, which differed in the number of PDZs. The constructs used for this purpose included the homotrimeric HtrA2 variants - full length wild type (WT or WWW) with a C-terminal His_6 tag, and the PDZ-deleted construct (N-SPD or ΔΔΔ) with an N-terminal maltose binding protein (MBP) fusion tag followed by a FLAG tag and a C-terminal His_3 tag (Fig. 1A). These proteins were purified separately from bacterial cells and were found to be ~99% pure, as estimated by SDS-PAGE. For generating the heterotrimers, purified WWW and ΔΔΔ trimers were mixed in equimolar concentrations and subjected to denaturing conditions. Since these homotrimers are stable at higher temperatures (Chaganti et al, 2013), the mild denaturation process promoted the dissociation of the trimers into individual subunits. Subsequent renaturation led to the formation of four plausible HtrA2 variant combinations - two homotrimers (WWW, ΔΔΔ) and two heterotrimers (WWΔ, WΔΔ) (Fig. 1A). Introduction of FLAG tag in ΔΔΔ construct helped in imparting difference in the pI of these variants (about ~0.2, as estimated by ProtParam software) (Gasteiger et al, 2005). Therefore, as expected, the variants in the renatured mixture were found to be well resolved in native PAGE in the order of decreasing pI values (Fig. 1B). Besides, the difference in the

number of FLAG epitopes further helped in confirming the identity of heterotrimers by Western blot. When probed with anti-FLAG antibody, three out of four bands (those containing the Δ subunit) were spotted with varying probe intensities; thus, confirming the distinctiveness of the heterotrimers (Fig. 1C). The individual HtrA2 variants were separated from the renatured mixture using a modified version of IMAC (Immobilized metal affinity chromatography), as differences in molecular weight and pI of the variants were minimal. As the C-terminal tag of each W or Δ subunit differed in the number of histidine residues, it altered the overall affinity of each renatured protein variant towards the resin and thus facilitated their separation. Small-scale batch purification was performed with elution buffers having a narrow imidazole gradient. ΔΔΔ eluted in the flow-through, followed by WΔΔ, WWΔ, and WWW eluting between 50-250mM imidazole gradient, as shown in Figure 1D. The heterotrimers obtained were stable, as estimated by native PAGE (Fig. 1E). The purity of WWΔ was found to be slightly lower (~90%) as compared to the other variants due to interference from the closely related variant WΔΔ, whose resolution of separation (~10%) from WWΔ fraction could not be further practically increased. Similar interference of ΔΔΔ was found in WΔΔ fraction. For further enzymatic studies, the homotrimers were purified, denatured and renatured separately.

Presence of single or multiple PDZ domains influences proteolytic activity of HtrA2

For understanding the effect of PDZ deletion on the overall residual activity and specificity of HtrA2 variants (homo- and hetero-trimers), time-based proteolytic cleavage assays were performed using saturating concentrations of the generic serine protease substrate β-casein. This well-established substrate has a putative binding site (GPFPIIV) that interacts with peptide recognition groove 'YIGV' of HtrA2 PDZ domain (Bejugam et al, 2013) and mimics the canonical allosteric modulation mediated by PDZ. It was observed that although the cleavage

pattern exhibited by all the variants was same (with three distinct bands resembling the cleaved products), the time taken to cleave β-casein differed significantly with removal of each PDZ domain from the trimeric ensemble (Fig. 2A). While variants having at least one PDZ domain (WWW, WWΔ and WΔΔ) cleaved within 10 min of incubation with a serial decline in the rate of cleavage with PDZ deletion, ΔΔΔ displayed significant reduction of activity with 100% substrate cleavage only by ~60 min (Fig. 2B). For obtaining enzyme kinetic parameters for these variants, quantitative fluorometric analysis was performed using varying concentrations of FITC-labeled β-casein as a substrate. It is interesting to note that despite reduction in the number of PDZ domains, WWΔ and WΔΔ exhibited enzyme activities greater than ΔΔΔ (Fig. 2C). In terms of V_{max}, a decreasing trend was observed with removal of each PDZ domain. WWW displayed the highest V_{max} value, followed by WWΔ and WΔΔ, which demonstrated approximately two-fold and four-fold decrease respectively (Table 1). Interestingly, the variant containing only Δ subunit (ΔΔΔ) showed ~10-fold decrease in V_{max}.

Although PDZ deletion resulted in only minor changes in the positive co-operativity of heterotrimers, the apparent sequential decline in the maximum velocity with removal of each PDZ domain proposes a strong possibility of intermolecular crosstalk between PDZ of one subunit with the adjacent protease domain, an event that eventually supports the second step of enzyme kinetics i.e. substrate catalysis. Alternatively, ΔΔΔ exhibited the maximum substrate binding affinity (K_m), followed by WΔΔ and WWΔ. This is expected as removal of the PDZ inhibition is known to open up the base of the pyramidal ensemble (Li et al, 2002; Martins et al, 2003), thereby increasing substrate accessibility and pseudo-affinity exhibited by enzyme towards the substrate. However, despite increased substrate accessibility, we observe a marked decrease in V_{max} and substrate turnover (k_{cat}) rates for WWΔ, WΔΔ and ΔΔΔ. These results, in

turn, not only hint toward the presence of malformed oxyanion hole in these PDZ-lacking variants but also corroborate very well with previous studies from our group (Bejugam et al, 2013; Chaganti et al, 2013). To assess the orientation of the oxyanion hole residues and capture the relative changes, comparative MD simulation analyses of these Δ-containing variants were performed for over 100 ns, keeping WWW as the reference structure. In-depth structural comparison revealed that there is a 90° anti-clockwise flip in the imidazole ring of F303 away from the catalytic triad residue H198 for WWΔ, WΔΔ and ΔΔΔ (Fig. EV1). This distal movement disrupts the nucleophilic exchange between F303 and H198 that is indispensable in stabilizing the negatively charged intermediates generated due to histidine-induced (H198) deprotonation of catalytic serine S306 (Bejugam et al, 2013; Singh et al, 2011). Presence of malformed oxyanion hole further explains the decrease in catalytic efficiencies of these variants, with ΔΔΔ showing approximately four-fold decrease, while WΔΔ and WWΔ approximately two-fold and ~1.5-fold decrease respectively, as compared to WWW. This also corroborates well with the time-based proteolytic assays, where although the cleavage pattern exhibited by all the variants was same, the amount of product formed by each variant differed with the reaction time points. Overall, these results suggest that apart from mediating the allosteric activation of HtrA2 upon substrate binding, all the three PDZs of the trimeric ensemble govern the enzyme activity by maintaining the catalytic triad orientation that is a prerequisite for a stabilized transition state formation and subsequent substrate catalysis.

Catalytic pocket reorientation and structural perturbation captured through MD simulation studies

To investigate the role of PDZ domain in modulating substrate accessibility, *in silico* docking analysis was performed using β-casein ligand peptide (GPFPIIV) and HtrA2 variants.

Comparison of the apparent binding affinities showed ΔΔΔ variant generating higher docking score (kcal/mol), compared to WWΔ and WΔΔ (Table EV1). Interaction analysis of the docked complexes revealed the propensity of the β-casein peptide (GPFPIIV) to bind with PDZ domain residues that include H394, P409 and G410 (Figs. EV2A, EV2B and EV2C). However, due to higher accessibility in ΔΔΔ, the peptide directly forms interactions with the active-site residues (H198, D228 and S306), resulting in higher binding score compared to the PDZ-containing variants (Fig. EV2D). Furthermore, to discern the underlying mechanism contributing to the difference in catalytic efficiency for all the HtrA2 variants, MD simulation analyses were performed with these docked complexes. Previous reports show that serine proteases like HtrA2 generally undergo conformational reorientation of the active-site residues (H198, D228 and S306) when an activator/substrate binds at the distant PDZ domain (Bejugam et al, 2013; Singh et al, 2011). This reorientation opens up the active-site pocket by moving H198 towards D228, and S306 away from the H198 residue. The conducted 1000 ns MD simulation of the β-casein bound HtrA2 variants also displayed similar catalytic triad reorientation. Comparative distance analysis with the unbound variant showed that in presence of β-casein peptide, the catalytic triad residues for WWW exhibit maximum movement, resulting in successful opening of the pocket. The most striking movement was observed in chain B, where the average distance between H198 and S306 increased from 4.1 Å to 5.3 Å (1.2 Å deviation) in presence of the peptide (Table EV2). Moreover, H198 and S306 residues of chain A and C also showed similar deviations of 0.8 Å and 1.0 Å respectively, which might further escalate the overall catalytic efficiency of WWW. However, with removal of PDZ, the opening of the catalytic pocket decreased gradually in WWΔ and WΔΔ (Table EV1). For peptide-bound WWΔ variant, the average distances between H198 and S306 residues in chain A, B and C were found to be 4.5 Å, 4.4 Å and 4.5 Å,

respectively, with an overall increment of 0.3 Å, 0.2 Å and 0.3 Å in comparison to the unbound WWΔ (Table EV2). In case of the WΔΔ variant, the movement seemed to be slightly lesser than that of WWΔ, where the highest deviation was of 0.2 Å in chain C (Table EV2). Although these movements enabled slight opening of the catalytic pocket for WWΔ and WΔΔ, the opening might not be sufficient to exhibit catalysis as efficiently as the WWW variant. This further explains the decrease in the catalytic efficiencies for WWΔ and WΔΔ, as observed in our aforementioned enzyme kinetics studies. The ΔΔΔ variant, on the other hand, showed closing of the catalytic pocket upon peptide binding, as the distance between the H198 and S306 was found to be decreased by 0.4 Å, 0.5 Å and 0.4 Å in chains A, B and C, respectively (Table EV2).

In addition to substrate-based activation, the apo-form of HtrA2 is also known to be activated by increase in temperature (Martins et al, 2003), with optimum activation temperature ranging between 45 °C to 55 °C (Chaganti et al, 2013). Hence, to investigate whether HtrA2 undergoes similar catalytic triad reorientation with temperature, the variants were subjected to MD simulation with temperature elevated from 300 K to 323 K. Similar to β-casein binding, temperature-induced activation also demonstrated a similar trend in opening of the catalytic pocket that decreased with deletion of PDZs. WWW variant showed highest deviation of 1.4 Å, whereas for WWΔ and WΔΔ, the maximum deviation was not more than 0.4 Å (Table EV2). However, as expected, ΔΔΔ variant demonstrated reverse movement of the active-site residues upon temperature induction that might have resulted in improper catalytic pocket formation.

For further extensive analyses and in-depth visualization of the underlying conformational changes, all the β-casein bound and temperature afflicted forms of HtrA2 variants were subjected to metadynamics MD simulation studies (Bussi & Laio, 2020). Generally, metadynamics analysis produces free energy landscape diagrams that segregate different conformations of a

system on the basis of overall free energy (ΔG) calculated over a collective set of variables; in this case, the distances among the catalytic triad residues. In presence of β-casein peptide as well as high temperature conditions, two separate conformations were evident for WWW, corresponding to their H198-S306 or H198-D228 distances. The two lowest conformations were observed at 1.6 kcal/mol and 1.5 kcal/mol, where the former ΔG value tends to reside at higher catalytic triad residue distances when bound to the activating peptide (Fig. 3A). The two separate lowest conformations of WWW at optimum catalytic pocket distances indicate that the opening up of catalytic pocket is a direct effect of the global conformational changes (Fig. 3B). Similar conformational changes have also been observed in WWΔ, where two discreet conformations at different free energy levels were evident (Figs. 3C and 3D). However, for WΔΔ, though there were a few separately placed conformations, distinct energy barriers among the conformations were missing, which is indicative of transient conformational changes that are not conducive toward enhancing its catalytic efficiency (Figs. 3E and 3F). Furthermore, in case of ΔΔΔ, single rigid conformation was observed indicating zero transitional state (Figs. 3G and 3H). This structural rigor might be due to the absence of any regulatory domain such as PDZ.

Intermolecular PDZ-protease crosstalk governs different activation modes for HtrA2

The final conformational changes in the different activation mechanisms for HtrA2, such as substrate-induced or temperature-based activation, have been proposed to be functionally similar and involve the displacement of PDZ domain to increase the accessibility to the active-site (Martins et al, 2003). However, none of the further studies provide a suitable validation for such hypothesis. From the aforementioned substrate-based enzyme kinetics studies and *in silico* MD simulation analyses, it is evident that extensive conformational changes with respect to PDZ movement are imperative for the activation of HtrA2 variants. In order to understand the role of

intra- and/or intermolecular crosstalk in allosteric induction, an activity-based chemical profiling using TAMRA fluorophosphonate (TAMRA-FP) was performed. TAMRA-FP is a widely recognized fluorescent probe that contains a fluorophosphonate moiety, which specifically labels the catalytic serine of an enzymatically active serine hydrolase through covalent modification of the side chain hydroxyl group (Liu et al, 1999). The linked TAMRA fluoropore (a fluorescein dye), on the other hand, facilitates detection through in-gel fluorescence imaging. The primary objective of this study was to confirm whether substrate binding and increase in temperature influence the active-site reactivity of the same attached protease domain (*cis*) and/or neighboring protease domains (*trans*) as well as to understand the variations in the conformational dynamics observed for both the activation mechanisms.

Substrate-induced activation mode

Upon activation by substrate, the extent of labeling of each subunit (W or Δ) by the fluorophore was efficiently determined through fluorescence-based SDS-PAGE experiments, as both the subunits have sufficient difference in their molecular weights (~10kDa). Since β-casein acts as a suitable PDZ-binding activator-cum-substrate, we performed the active-site chemical profiling assay in presence of this protein. Our results demonstrate that neither WWW nor ΔΔΔ subunits were TAMRA-labeled in their basal states (Fig. EV3A), as expected. The modification is absent in WWW, as it might be restricted due to over-crowding of PDZs in the absence of the substrate. However, interestingly, the unbound forms of WWΔ and WΔΔ exhibited visible TAMRA fluorescence for each subunit (Fig. EV3A) as compared to the homotrimers. For the unbound WWΔ and WΔΔ variants, the W subunit showed ~2.4- and ~1.8-fold increase respectively, while the Δ subunit exhibited ~2.8- and ~5.3 fold respectively suggesting occurrence of favorable conformational changes in and around the active-site of adjacent Δ subunit(s) with removal of

one or two PDZ domains (Fig. EV3C). On the other hand, in presence of β-casein, WWW showed highest fluorescence labeling, while ΔΔΔ exhibited minimal fluorescence (Fig. EV3A). This confirms that binding of a C-terminal activator to PDZs engages this regulatory domain and greatly alters the active-site reactivity of the entire trimeric ensemble. Interestingly, comparison of WWΔ and WΔΔ shows greater TAMRA-mediated modification in Δ subunit of WWΔ than the other variant (Fig. EV3C). This might be attributed to the presence of two PDZ domains from the respective W subunits in WWΔ, which together influence the active-site reactivity of a single Δ subunit through an intricate intermolecular PDZ-protease interplay. In WΔΔ, although the PDZ-crowding is less, the lesser fluorescence equates to modification of two Δ subunits with a single PDZ. These observations ascertain presence of a predominant *trans* PDZ-protease crosstalk within the trimeric ensemble of HtrA2 that helps modulating the allosteric activation upon substrate binding. To demonstrate this more explicitly, quantitation of the TAMRA-FP intensities was performed and compared with respect to their corresponding basal states so as to determine the fold change in active-site modification in presence of the substrate (Table EV3A). While the bound WWW variant represents 11-fold increase in TAMRA fluorescence compared to the unbound form, the W subunit of substrate-bound WWΔ and WΔΔ exhibit five- and four-fold increase respectively (Fig. 4A). Interestingly, each PDZ-lacking monomeric subunit (Δ) of these heterotrimeric variants, WWΔ and WΔΔ demonstrates increase in activity by seven- and three-fold respectively compared to their unbound forms (Fig. 4A), thus suggesting dependence of the TAMRA-modification of the Δ subunit on the total number of engaged PDZs present in a particular variant ensemble. The observed 2.5-fold increase in fluorescence in the bound ΔΔΔ compared to unbound form might be due to greater accessibility of the active-site to the substrate

as a consequence of lack of surrounding PDZ domains. This hypothesis is substantiated by the enzyme kinetics studies that showed lower K_m value for this variant of HtrA2.

Taken together, data from multiple independent studies affirm occurrence of *trans*-mediated allosteric communication between the ligand-bound PDZ of one subunit with the protease domain of the adjacent subunit. The extent of TAMRA-FP labeling of the Δ subunits in the heterotrimers - WWΔ and WΔΔ provide strong evidence that this intermolecular crosstalk is extremely essential for altering the active-site environment of adjacent subunits towards a more catalytically competent state.

Temperature-based activation mode

For understanding the plasticity at the PDZ-protease interface upon heat activation, enzyme-modification assays using TAMRA-FP was carried out by incubating each variant at 50 °C, a temperature at which both WWW and ΔΔΔ are known to remain structurally stable and exhibit increased proteolytic activity (Chaganti et al, 2013) (Figs. EV3B and EV3D). Here we see some interesting changes in fold-increase in active-site modification among different variants. Although the W subunit in WWW showed maximum modification amongst all other W subunit-bearing variants, the difference in activity fold-change with respect to the basal state in WWW, WWΔ and WΔΔ were quite comparable (Fig. 4B and Table EV3B). Strikingly, the modification of Δ subunit in each variant was found to be inversely proportional to the number of PDZs present in the variant ensemble, with ΔΔΔ exhibiting maximum change in the heat-induced activation. This apparent behavioral anomaly might be attributed to the difference in the structural dynamism of the protease in these two distinct modes of activation. While substrate binding at the distal allosteric site engages the PDZ(s) that sequentially opens up the ensemble

and further bring about active-site rearrangement, the heat-activation model is primarily dependent on increased plasticity of the PDZs in the trimeric ensemble. With increase in temperature, the overall kinetic energy of the ensemble increases that might lead to enhanced movement at the regulatory loop regions and the flexible PDZ-protease interface. With no substrate-mediated conformational changes, the mechanism plausibly relies predominantly on the room available in the three-dimensional space for free movement (spatial dynamism) of the PDZ domains. Thus, while WWW and WWΔ experience substantial steric hindrance from the adjoining PDZs, the single PDZ domain of WΔΔ remains relatively free to modify the adjacent Δ subunits. In ΔΔΔ, however, the increase in activity might correlate with opening up of the active-site as a function of heat, which corroborates well with the MD simulation analysis (Fig. 3H). This inference is strengthened by the structural data (described below) where the active-site rearrangement is observed due to increased dynamics of the regulatory loops that are found to be more disordered in the crystal structure. Furthermore, these interpretations support a previous FRET-based intramolecular PDZ-protease interaction study, which suggested that PDZ movement with respect to the protease domain follows a V-shaped trajectory upon increase in temperature (Chaganti et al, 2013). Overall, these results hint towards a heat-activated *trans*-mediated allosteric communication, where increase in temperature induces rearrangement of the catalytic triad by substantially opening up the ensemble, and increasing substrate accessibility.

Trans **PDZ-protease crosstalk predominates the allosteric communication in HtrA2**

To further support the chemical profiling studies and determine the effect of ligand-bound PDZ domain(s) on the active-site of the protease in *cis* and/or *trans* subunit(s), we generated heterotrimeric HtrA2 variants that differed in the number of active-site serine (S306) residue(s) in parallel with the PDZ(s). To develop such variants, we replaced S306 with alanine (hereafter

denoted as 'I') in WWW and ΔΔΔ variant constructs. Combining one of these inactivated homomers with the corresponding active homomer, we generated four different heterotrimeric combinations - $W_IW_I\Delta$, $W_I\Delta\Delta$, $WW\Delta_I$ and $W\Delta_I\Delta_I$. Comparison of enzymatic parameters of these engineered protease combinations i.e., $W_IW_I\Delta$, $W_I\Delta\Delta$, $WW\Delta_I$ and $W\Delta_I\Delta_I$ with their corresponding active counterparts (WWΔ and WΔΔ) depict reduction in the rate of β-casein substrate cleavage. Interestingly, despite presence of two active-sites contributed by each Δ subunit in $W_I\Delta\Delta$, this heterotrimeric complex cleaved ~90% of the substrate in 30 min; while $W_IW_I\Delta$ (with a single active-site in Δ) showed higher activity by cleaving the entire substrate approximately within the same time span (Fig. 5A). This is in contrast with the results observed for WΔΔ and WWΔ, where both the active variants completely cleaved the substrate within 15 min. Quantitatively, our data demonstrates that while $W_IW_I\Delta$ exhibits similar enzymatic parameters as WWΔ (Fig. 5B), there is a marked 1.5-fold decrease in the V_{max} and turnover rate values of $W_I\Delta\Delta$ with respect to WΔΔ (Table 1). Furthermore, an enhanced substrate binding affinity is observed in $W_I\Delta\Delta$, and higher apparent co-operativity in both $W_IW_I\Delta$ as well as $W_I\Delta\Delta$. The catalytic efficiencies of both these variants, $W_IW_I\Delta$ and $W_I\Delta\Delta$, are slightly lesser than their active counterparts. Interestingly, the catalytic efficiency of $W_IW_I\Delta$ is ~1.5-fold greater than that of $WW\Delta_I$, thus strongly ascertaining the existence of *trans*-mediated allosteric communication via the PDZ domains. Moreover, $WW\Delta_I$ exhibited similar catalytic efficiency as that of $W\Delta_I\Delta_I$, despite having two active-sites in subunits with intact PDZs. These results suggest that the number of active-sites within the trimeric ensemble is not the primary defining factor for the total residual activity of the enzyme. This is conceivably because the loss of active-sites is very well compensated by PDZ-mediated conformational changes that might be necessary for a well-formed oxyanion hole and subsequent substrate catalysis. In both, substrate- and heat-induced

activity-based chemical profiling assays, the Δ subunit in $W_IW_I\Delta$ showed slightly greater modification by TAMRA than $W_I\Delta\Delta$. Thus, similar observations from two distinct and independent studies strongly hint towards adoption of a unique compensatory mechanism, where the single/double PDZ domain(s) strive(s) to indemnify the loss of activity of the attached subunit(s). This is achieved by substantially increasing the proteolytic activity of the adjacent active subunit(s), so as to preserve the total residual activity of the entire ensemble. Taken together, these results evidently prove the existence of a strong *trans*-mediated allosteric communication within the HtrA2 trimer via the coordinated movement between all the three PDZs that eventually governs the proteolytic activity of the entire multimeric protein complex (Fig. 5C).

Removal of PDZ affects the secondary structural elements of the trimeric assembly

For understanding the role of PDZ deletion on the overall structural integrity of HtrA2 ensemble, we crystallized the catalytically inactive ΔΔΔ variant (S306A) of HtrA2 (PDB ID: 7VGE) and determined the structure at 4 Å resolution (Table 2). Considering the fact that HtrA2 followed the trend of other family members, which also showed relatively lower resolution (~3 Å) of their PDZ-deleted structures, it can be inferred that it might be due to the inherent dynamism and reduced compactness of the protease without PDZ. The asymmetric unit for the current structure contained six Δ subunits assembled into two discrete trimeric ensembles (chains - ABC and DEF). These two ensembles are stacked against each other in a non-superimposable tail-to-tail arrangement (Fig. 6A), resulting in occlusion of the funnel-shaped solvent-accessible surface that generated a buried surface area of 12610 $Å^2$. The structure further demonstrated that the subunits of each trimer are symmetrically packed around a three-fold molecular axis that together provide an inclusive view of six individual Δ subunits, with each subunit exhibiting slight variations in

the catalytic triad and loop regions. The overall trimeric structure is comparable to the reported full-length HtrA2 (PDB ID: 1LCY) with root mean square deviation (RMSD) value of <0.45 Å for main-chain backbone atoms. Each Δ subunit displayed structural deviations near the activation domain as well as other regulatory loops as compared to 1LCY. Superposition of the structures reflects absence of the sensor loop L3 in both 1LCY and ΔΔΔ. It is to be noted that although certain regions of the activation and regulatory loops in different subunits of ΔΔΔ could not be built due to relatively lower resolution of the electron density, the activation domain loops viz. LA (residues 170-174) in Chain D and L2 (residues 323-329) in Chains A and C could be successfully constructed.

Inter-trimer interactions and interface analyses

Interface analysis pertaining to trimer-trimer interactions revealed that LA loop from each subunit of the upper trimer (ABC) stabilized the corresponding LA loop from the alternate subunit of the trimer at the bottom (DEF) (Figs. 6B and EV4A). This might be the plausible reason for the two trimers to co-exist in a single asymmetric unit during crystal packing. Since PDZ domains are spatially close to the corresponding LA loops in the full-length structure, we speculate that absence of PDZ (especially β15-α6 region) affects the stabilization of LA loop in the ΔΔΔ variant. The association of two trimers might be essential in the stabilization of highly dynamic LA loop, as seen in Chain D. In addition, the inter-trimer interactions in ΔΔΔ are mostly non-bonded contacts between residues of LA and LD loop. Moreover, the non-bonded interactions between chains A and D (few residues resolved) are mediated primarily through the L2 loop residues (324-327), which are present in the inner core of the trimer association. Thus, LA, LD and L2 loops might play important roles in association of the two trimers in the crystal asymmetric unit of the ΔΔΔ variant.

Structural comparisons and subunit interaction analysis

Notably, LA loop in chain D of ΔΔΔ assumed a disordered conformation in contrast to the extended anti-parallel β sheet (β1and β2) as observed in 1LCY (Fig. 6C). On the other hand, β7 gained an extended β-sheet conformation with respect to the positioning of the regulatory loop LD in ΔΔΔ as compared to 1LCY (Figs. 6C and EV4C). With regards to L2 loop, a set of amino acids (M323, V325, I329, F331) from the β11-β12 region have been reported to interact with some residues (M365, L367, I373, L377) residing in the α5 and β14 elements of PDZ domain in the full-length protein (Li et al, 2002). Due to the lower structural resolution, absence of a few residues from the L2 loop in most of the subunits (except chains A and C) might be attributed to the missing PDZ domains in the ΔΔΔ variant (Figs. 6C and EV4B). This deletion might have adversely affected the protein stability by abrogating a series of intramolecular hydrophobic contacts between the protease and PDZ domain that subsequently culminate in a disordered L2 loop with enhanced plasticity. Although the intermolecular salt bridges in most of the Δ subunits are similar to the wild type structure as observed in 1LCY, deletion of PDZ also affected the number of intramolecular salt bridges in the ΔΔΔ variant. Interestingly, in most of the subunits, one of the conserved salt bridges between D190 (OD2) and R233 (NH2) remained intact despite PDZ deletion in the ΔΔΔ variant, thus underscoring its importance in maintaining the intramolecular integrity of HtrA2 subunits. The structure depicts that all the disordered regulatory loops i.e., LA, L2 and LD are poised close to the catalytic triad residues, H198, D228 and S306 in both wild type (1LCY) and the ΔΔΔ variant (A306 in both the crystal structures). However, in the latter, while retaining similar orientations in most of the Δ subunits, these residues are comparatively more exposed. Deletion of PDZ also breaks the inter-subunit hydrogen bond between Y147—Q146 at the N-terminus region. Thus, PDZ deletion can also be

said to have a significant influence on the conformational orientation of N-terminal region of each subunit within the trimeric ensemble.

Furthermore, structural comparison of this variant with relatively active bacterial counterpart, $DegS^{\Delta PDZ}$ (PDB ID: 3LGI) demonstrated several significant differences in the movement of regulatory loops (RMSD <2.9 Å). Although there were no prominent changes in the orientation of the catalytic triad residues between the two structures, major differences existed in the orientation of loops LA, LD, L2, L3 and their associated secondary structures (Fig. 6D). Interestingly, majority of the ΔPDZ structures of HtrA family displayed presence of more than one trimer molecule in the crystal asymmetric unit. Although it is unclear whether deletion of PDZ affects the crystal packing (as implicated through lower resolution of crystal structure) in a way that it now has to accommodate more than two protein molecules plausibly to stabilize the structure, however, if this scenario holds true, then it would ascertain the involvement of even protease domains in the higher-order oligomer formation rather than the sole contribution of inter-trimer PDZ-PDZ interactions (Toyama et al, 2021). Taken together, perturbations in the appropriate secondary structure formation of the activation domain and the regulatory loops near the catalytic triad seem to be the major reason for significant decline in enzyme activity in ΔΔΔ. These structural analyses are in concurrence with our functional assays, thereby highlighting the importance of PDZ domains in restructuring the orientation of regulatory loops near the ΔΔΔ catalytic triad.

DISCUSSION:

Unlike its bacterial homologs and other human counterparts, regulation of the mitochondrial serine protease HtrA2 occurs at multiple stages of activation plausibly to safeguard untimely

proteolysis of its wide array of substrates. Despite numerous efforts to decipher the innate intricacies behind its regulation, both discrete and collective roles of HtrA2 subunits in promoting the allosteric coordination within the trimeric ensemble remained abstruse till date. Although, each subunit of human HtrA proteins contains a single PDZ (unlike their bacterial counterparts), the modes of PDZ-mediated regulation vary significantly even within human HtrAs suggesting evolutionary diversification of the protease structure across and within species to cater to distinct functional requirements. While a plethora of research efforts have highlighted the importance of allosteric modulation of HtrA2 from a global perspective (Chaganti et al, 2013; Gieldon et al, 2016; Li et al, 2002; Martins et al, 2003; Merski et al, 2017b; Singh et al, 2014; Toyama et al, 2021), the minutiae of the intricate intra- and inter-subunit network involving the regulatory PDZ domains remain unperceived. Therefore, in this study, we have adopted a unique multidisciplinary approach to demonstrate the mechanism of PDZ-mediated synergistic coordination among different domains and subunits of the trimeric protease ensemble. Using protein engineering, we have devised a strategy to obtain HtrA2 variants with decreasing number of PDZ domains in the trimeric ensemble, so as to elucidate how individually and/or in unison this protein-protein interaction domain regulates *cis*- and/or *trans*-mediated protease activation. Our observations showcase that although the sequential deletion of PDZs does not affect the overall pattern of cleaved product formation, it significantly reduces the rate of proteolysis. While earlier crystallographic reports of HtrA2 and bacterial DegS hint towards inhibitory role of PDZ, our enzymological data show a decreasing trend in the substrate cleavage rate with sequential reduction in the number of PDZs. This underscores the contribution of PDZ domain(s) toward active-site rearrangement in a manner that is conducive toward efficient protease functions. Interestingly, in contrast to DegS, where the basal activity is inversely

proportional to the number of PDZs in the trimer, our findings demonstrate positive regulation of HtrA2 enzymatic functions by this regulatory C-terminal domain. Furthermore, our study reiterates that sequential removal of PDZs from the HtrA2 trimeric ensemble adversely affects its thermal stability (Chaganti et al, 2013) (data not shown). Thus, apart from solely playing an inhibitory role and upholding the inactive state when unliganded, PDZs in HtrA2 might also be responsible for maintaining the stability of the active trimer as well as facilitate a coordinated relay of allosteric information among the neighboring subunits upon ligand binding in a precise manner. Moreover, the decline in the substrate-induced proteolytic activity of the heterotrimers harboring one or two PDZs (WWΔ and WΔΔ) strongly suggests that the contribution of each subunit towards the total residual enzyme activity is defined by the structural identity of both the neighboring subunits, and that the subunits together exist in a cooperatively-shared energy landscape.

The structural intricacy in HtrA family has often complicated the understanding of their mechanisms and hence, presence of multiple contradicting reports on their allosteric modulation is not unanticipated. For example, in DegS, while remodeling of the active-sites by the neighboring counter-clockwise ligand-bound subunits (Clausen et al, 2011; Hasselblatt et al, 2007; Wilken et al, 2004) is one plausible mechanism, other groups highlight OMP peptide mediated activation of substrate proteolysis in both the *cis*- and *trans*-protease domains, with a predominant *cis* PDZ-protease interaction governing the overall DegS activity (Mauldin & Sauer, 2013). Similarly, despite the structural studies (Li et al, 2002) implicated inhibitory role of PDZ in HtrA2 activity, Chaganti *et. al.*, (Chaganti et al, 2013) hinted towards a *trans* PDZ-protease crosstalk-mediated reorganization of the active-site loops that leads to a catalytically competent oxyanion hole formation. Therefore, to validate this finding as well as quantitatively

depict the contribution of individual PDZ(s) in allosteric regulation of HtrA2, we performed active-site chemical profiling using fluorescent probe TAMRA-FP in the present study. Our data provides a very unique and interesting revelation where the substrate-unbound wild type HtrA2 with all PDZs intact exhibits basal or minimal activity. On the contrary, sequential deletion of PDZs in WWΔ and WΔΔ equates to formation of a conducive substrate-binding site at the basal state, while deletion of all the PDZs (ΔΔΔ) leads to no active-site modification. Thus, the basal state in HtrA2 wild type represents a protective mechanism to prevent unwanted protease activation under normal cellular conditions. However, the increase in active-site modification in the heterotrimeric variants strongly implies that absence of one or two PDZ domains (similar to ligand-bound PDZs in cellular environment) might provide an opportunity to the adjacent subunit with intact PDZ(s) to have greater access to the PDZ-lacking subunit, thus allosterically modifying its active-site and preparing it for subsequent substrate binding. The very crowded trimeric ensemble in the apo-HtrA2 wild type does not provide much room for such dynamic behavior and hence, might be energetically unfavorable for catalysis. This string of riveting information simulates a precisely controlled concerted mechanism of HtrA2's mode of action in the cellular milieu, which might be critical towards maintaining its specificity while participating in several pathways involving a wide repertoire of substrates. In addition, the active-site modification studies in presence of a C-terminal ligand firmly indicate a *trans*-mediated allosteric activation of serine protease HtrA2 by its distal PDZ domains. Similar studies that have been replicated with heterotrimers lacking one or more active-site serine residues ($W_IW_I\Delta$, $W_I\Delta\Delta$, $WW\Delta_I$ and $W\Delta_I\Delta_I$), along with quantitative enzyme kinetic analyses, decidedly substantiate our claim. Besides, in our previous temperature-based fluorescence quenching studies, no changes in the K_{sv} (Stern-Volmer) constant for the full-length monomeric variant

(F149D) signified the requirement of the trimeric ensemble and hypothetically suggested that PDZ might not be involved in intramolecular active-site rearrangement. Through this present study, we demonstrated that both substrate- or temperature-induced activation of HtrA2 occurs via a concerted *trans*-mediated intermolecular PDZ-protease crosstalk within the trimeric ensemble. However, the observed distinct behavior of the heat-based activation might be attributed to the overall dynamism accrued by the PDZs due to increase in temperature. With removal of the PDZ inhibition (as in ΔΔΔ), activation via temperature might cause certain favorable rearrangements at the N-terminal region (Chaganti et al, 2013) and around the active-site such that it compensates for the lost PDZ domains by opening up the ensemble substantially. Moreover, these observations accentuate the role of the C-terminal regulatory domain in overall protease activity in a cooperative and stepwise manner, which is also evident from our enzyme kinetic parameters as well as from a recent NMR study (Toyama et al, 2021).

To resolve the ambiguities regarding the role of PDZ domains in the activation mechanism of HtrA2 and ΔΔΔ (Bejugam et al, 2013; Chaganti et al, 2013; Jarzab et al, 2016; Li et al, 2002; Martins et al, 2003; Singh et al, 2014; Toyama et al, 2021), we reported the structure of catalytically inactive (S306A) version of ΔΔΔ. The structure highlighted that although the accessibility to the ensemble core is increased and the active-site triad residues (H198, D228 and A306) are more exposed than that in the full-length protein, there is increased disorderedness and lack of secondary structure formations around the important regulatory loops with deletion of all three PDZs. As the ΔΔΔ and wild type (PDB ID: 1LCY) structures share similar orientation of catalytic triad residues, we believe that increase in temperature or the binding of specific ligands (activator or substrate) greatly influences the PDZ dynamics and subsequently the active-site reactivity by bringing about suitable rearrangements of the regulatory loops with respect to the

oxyanion hole. This is a crucial step in shifting the equilibrium from inactive to active state (E to E*). For DegS, which is a more open ensemble, and where PDZs act as inhibitory modules, the $DegS_{\Delta PDZ}$ variant is found to be in an active conformation and therefore, deletion of PDZs do not greatly affect the catalysis of this variant (Sohn et al, 2007; Sohn et al, 2010; Walsh et al, 2003). On the contrary, PDZs in HtrA2 seem to play a greater role in structural stabilization of the entire ensemble by assisting the secondary structure formation in protease domains, especially around the regulatory loops that together form the activation domain. The ΔΔΔ structure clearly shows that loss of the C-terminal PDZ domain disrupted the formation of the additional intramolecular interaction networks between the protease domain (β11-β12) and PDZ domain (α5 and β14), which otherwise are required for stabilization of the trimeric ensemble in a closed conformation. These same regions of the PDZ (strand β-14, along with the α-5 and α-7 helices) are also known to form the peptide-binding cleft (Zhang et al, 2007). Thus, in the absence of any form of activation, PDZs help to maintain the pyramidal architecture of HtrA2 in a closed conformation by stabilizing intramolecular PDZ-protease domain interactions within the trimeric ensemble. The full-length and the PDZ-deleted structure of HtrA2 differ in their interaction networks, especially intramolecular salt bridges and intermolecular hydrogen bonds. Thus, absence of inter- and intra-subunit interactions in the ΔΔΔ variant, which could have otherwise favorably assisted establishment of the required transitions (L3 to LD* loop via L1*/L2* (asterisk denotes adjacent subunits)) to the catalytically competent state (Bejugam et al, 2013), and also energetically stabilized the entire trimeric ensemble, reiterates the indispensability of these regulatory domains in upholding the overall protease structural integrity and functions.

Overall, our observations from multiple independent yet complementary studies propound a working model for HtrA2 activation, where the initial step of ligand binding or increase in

temperature enhances the competence of the apo-enzyme by shifting the intrinsic equilibrium from an inactive state (E) to a higher affinity conformation (E') that eventually promotes a more catalytically competent state (E*) through a synergistic *trans* PDZ-protease coordination, as elaborated in Figure 7. Briefly, binding of ligand at the exposed substrate binding pocket of the PDZ brings about subsequent conformational changes at the PDZ-protease domain interface that are different from the original inactive state. The primary binding leads to displacement of a single PDZ (E_S' state), which further commences the synergistic coordination and formation of new interaction networks between the PDZ and protease domains of adjacent subunits, subsequently increasing the affinity of other subunits towards the ligand by opening up the ensemble as well as reorienting the catalytic triad for enhanced catalysis. On the other hand, apart from substrate-induced PDZ dynamics, temperature-mediated mode of activation is also influenced by the overall stereochemical contour of the surrounding three-dimensional space (Fig. 7). Here, increase in temperature leads to inter-domain PDZ movement in a way that not only reduces the steric crowd but also leads to subtle distal conformational changes conducive toward competent active-site formation. Thus, under cellular conditions, stress-related temperature change might induce initial opening of the PDZs, in turn making the catalytic pocket more accessible for substrate binding and proteolysis. Furthermore, this temperature-induced reordering of the active-site (E_T' state) might be particularly important in scenarios where the protease-domain defines initial substrate binding and its subsequent cleavage (unpublished data). Thus, this model describes an energy landscape that might be allosterically tuned in multiple ways to help the protease to conform to different cellular requirements for optimal biological leverage. This kind of dynamic perpetuity, observed in a multimeric protease ensemble through a discrete and sequential inter-domain coupling, allows a robust coalescence of regulatory

strategies amongst heterogeneous sub-ensembles that successfully culminate in an amenable functional conformation (Motlagh et al, 2014).

In conclusion, this manuscript unequivocally describes the activation mechanism of HtrA2 at the atomic level using a unique retrospective approach through dissecting and rebuilding the protein structure. This is the first report that describes *trans*-mediated allosteric activation of HtrA2, while highlighting the role of individual domains of each subunit of the trimeric ensemble. Therefore, this study might open up new avenues for devising tailor-made strategies toward modulating HtrA2 functions with desired characteristics for therapeutic benefit. Most importantly, delineation of this multidimensional allosteric model system that amalgamates both activation and stabilization of the macromolecular ensemble through an intricate intermolecular crosstalk for transmission of information within and outside cellular pathways provides an advanced understanding of allostery in general from a more quantitative perspective.

MATERIAL AND METHODS:

Recombinant protein expression and purification

The mature form of HtrA2 full length protein, comprising residues 134–458, is considered as Wild type (WT or WWW) and the PDZ lacking HtrA2 variant containing the N-terminus-SPD domain (residues 134-210) is considered as N-SPD or ΔΔΔ. These proteins are cloned and expressed in pET-20b (Addgene, Cambridge, MA, USA) and modified pMAL-c5E vectors (New England Biolabs, Ipswich, MA, USA) respectively, as previously described (Chaganti et al, 2013). The latter had a TEV (Tobacco Etch Virus) protease cleavage site introduced for removal of the fusion tag. An additional FLAG octapeptide (DYKDDDDK) tag at the N-terminal end in

ΔΔΔ construct and single amino acid substitution of S306 residue to Alanine in both the constructs (WWW and ΔΔΔ) was performed using site-directed mutagenesis (Stratagene, Austin, TX, USA). The insertion and point mutations were verified by automated DNA sequencing. Recombinant proteins were expressed in *E. coli* BL21 (DE3) pLysS and Rosetta (DE3) pLysS strains (Novagen, Billerica, MA, USA). These cells were grown at 37 °C until the optical density at 600 nm reached ~0.6 AU and the protein expression was then induced by adding isopropyl β-D-1-thiogalactopyranoside (IPTG) to a final concentration of 0.3 mM. The cells were further cultured at 18 °C for 18 h post induction and then harvested for protein production. Protein variants with a C-terminal Histidine tag were purified by affinity chromatography using Ni-NTA resin (Nucleo-pore, Genetix Biotech Asia Pvt. Ltd), while those with N-terminal maltose binding protein (MBP) fusion tag were purified using amylose resin (New England Biolabs). All the protein variants were purified in buffer A (20 mM Na_2HPO_4/NaH_2PO_4 (pH 8.0) containing 100 mM NaCl and 3% (v/v) glycerol) and the proteins obtained were >95% pure, as estimated by SDS PAGE.

Generation and purification of heterotrimeric HtrA2 variants

For obtaining heterotrimeric variants, the use of simultaneous heat and chemical denaturation process was employed. Purified WWW and ΔΔΔ trimers were mixed in equimolar concentrations and diluted up to 15-fold in buffer A, additionally containing 6 M guanidinium chloride (pH 8.0). This reaction mixture was further subjected to heat by incubating at 50 °C for 1-2 h for efficient denaturation into monomeric subunits. The solution was further dialyzed extensively against a renaturation buffer (buffer A (pH 8.0) containing 300 mM arginine with varying content of glycerol) at 4 °C. The final step involved dialysis in buffer A (to remove arginine) and concentrating the renatured protein mixture using an Ultracel-30k centrifugal filter

(Merck Millipore). For further separation of the different HtrA2 variants (homo- and hetero-trimers), this renatured mixture was bound to Ni-IDA column pre-equilibrated with buffer A. Since the variants differed in the total number of histidine residues (WWW-His_6 and ΔΔΔ-His_3) at their C-terminal end, a very shallow gradient of imidazole (10-250 mM) in the elution buffers was used for their separation. The impurities eluted in the flow-through fraction and up to 30 mM imidazole buffer washes, followed by WΔΔ, WWΔ and WWW eluting between 30 – 250 mM imidazole containing elution buffers. The elution fractions were loaded on SDS PAGE for analyzing the fractions containing the heterotrimers.

Native PAGE and Western Blot

To confirm the identity of the generated HtrA2 heterotrimers, protein samples from the appropriate purification fractions were mixed with native PAGE sample buffer (62.5 mM Tris-Cl, pH 6.8, 15% glycerol, and 0.01% bromophenol blue) and loaded on 7.5% native PAGE. The gels were run at a constant voltage of 50 V for 5 h at 4 °C and were analyzed by Coomassie Blue staining. Since all the homo- and hetero-trimers also differed in the number of FLAG tag (originally introduced in ΔΔΔ construct), the unstained native PAGE gel was additionally probed with monoclonal anti-FLAG antibody by performing Western blot. The separated protein bands were transferred on nitrocellulose membrane (Millipore, Italy) using Invitrogen wet transfer mini blot module (Thermo Fisher Scientific, USA) in 1X transfer buffer (25 mM Tris, 192 mM glycine, 20% (v/v) methanol, 0.025–0.1% SDS, pH 8.3) at a constant voltage of 15 V for 60-90 min. The membrane was then blocked with 5% bovine serum albumin (BSA) prepared in 1X TBST buffer (Tris-buffered saline (TBS) containing 0.1% Tween-20) for 1h, followed by overnight incubation with 1:2000 dilution of anti-FLAG antibody (Sigma Aldrich) at 4 °C. The membrane was further incubated at room temperature with 1:5000 dilution of goat antimouse

IgG HRPO (Sigma Aldrich) secondary antibody for 1 h. After each incubation period mentioned above, the membrane was washed three to six times with 1X TBST solution. Antibody dilutions were prepared in TBS containing 0.01% Tween-20 and 1% BSA. Bands were developed using an enhanced chemiluminescence kit (Thermo Fischer, USA).

Protease assays

Protease activity of different HtrA2 variants (homo- and hetero-trimers) was semi-quantitatively determined using the generic serine protease substrate β-casein (Sigma, St. Louis, MO, U.S.A.). For each 30 µl reaction, 2 µg of respective protein variant was incubated with 6 µg of β-casein in buffer A at 37 °C for a course of different time points (0-90 min). The reaction was stopped with a 5X SDS sample loading buffer, followed by boiling for 10 min. The cleavage products were resolved on 15% SDS PAGE and the results were analyzed by Coomassie staining. Protein bands were quantitated using *GelQuant.NET* software. The data was normalized with respect to the uncleaved substrate control and was plotted using the GraphPad Prism 5 (GraphPad Software, San Diego, CA, USA). For all quantitative studies, fluorescein isothiocyanate (FITC) β-casein (Sigma, St. Louis, MO, U.S.A.) was used as the substrate. For each 100 µl reaction mixture, 2 µM protein was incubated with increasing concentrations (0-20 µM) of FITC β-casein at 37 °C in buffer A. The rate of proteolytic cleavage was monitored in Cytation™ 5 multi-mode plate reader (BioTek Instruments, Inc.) using an excitation wavelength of 485 nm, followed by emission at 535 nm. For each HtrA2 variant, the initial velocities V_0 (µM/min) were calculated using linear regression analysis. The steady-state kinetic parameters were calculated from the reaction rates by fitting the data to the Hill form of Michaelis–Menten equation, Velocity = $V_{max}/[1 + (K_{0.5}/[\text{substrate}])^n]$ (where V_{max} represents the maximum velocity and $K_{0.5}$ is the substrate concentration at half maximal velocity) in GraphPad Prism version 5.01 for Windows

(GraphPad Software, San Diego, California USA). All the experiments were performed independently in triplicates and the mean SEM values were reported.

Activation assay using chemical probe

For trapping the active-site reactivity, chemical profiling of the enzyme activity was performed using ActivX TAMRA-FP Serine Hydrolase Probe (Thermo Scientific, USA). 0.1mM stock of TAMRA-FP was prepared by dissolving the commercially available probe in anhydrous dimethyl sulfoxide, according to the manufacturer's protocol. For each reaction mixture, a final concentration of 2 µM probe was added and the reactions were incubated for 30 min. For substrate-based and temperature-induced activation, the incubation temperatures were set to 37 °C and 50 °C respectively. The reactions were terminated by adding 5X SDS sample loading buffer, followed by boiling for 10 min. The labeled proteins were resolved on 15% SDS PAGE and the results were analyzed using ChemiDoc™ MP Imaging System (Bio-Rad laboratories, Inc.) with Cy®3 filters. For better quantitative analysis, the fluorescence intensities of each subunit band were measured using Image Lab™ - version 6.0.0 build 25 (2017, Bio-Rad laboratories, Inc.) and the fold change between the intensities of the subunits in the test samples with respect to their corresponding controls were then plotted for graphical representation.

***In silico* preparation of the heterotrimeric models of HtrA2**

For preparation of *in silico* heterotrimeric models, three-dimensional (3D) crystal structure of HtrA2 (PDB ID: 5M3N) was retrieved from Protein Data Bank (Merski et al, 2017a). The 3D structure lacked crystal information for few loop regions- an N-terminal loop (^{1}AVPSPPPA^{8}), a loop in the SPD region (^{280}RPARDLGLPQTNV^{292}) and the linker region (^{344}RGEKKNSSSGISGS^{357}) (Merski et al, 2017a). Hence, these missing regions were modeled

using *ab initio* mode of loop filling and protein preparation programs in Prime (Prime, Schrödinger, LLC, New York, NY, 2020) (Jacobson et al, 2004). Loop filling was done on the basis of permissive dihedral angle values for different residues, followed by repetitive rounds of sample loop clustering, optimizing the side-chain, and energy minimization of the loops (Jacobson et al, 2004). The resultant loop-filled wild type HtrA2 monomer was energy minimized using Desmond (Desmond, Schrödinger, LLC, New York, NY, 2020). Using the crystal symmetry data of HtrA2 monomer (Merski et al, 2017a), the trimeric ensemble of HtrA2 wild type (WWW) was generated, which was further modified by deletion of the linker and PDZ domain in subsequent chains, viz, WWΔ (with linker and PDZ deleted in chain C), WΔΔ (with linker and PDZ deleted in chain B and C), and, ΔΔΔ (with linker and PDZ deleted in all the three chains). These models were then subjected to docking using a β-casein peptide denoted by GPFPIIV (a generic substrate). Docking was performed using Bioluminate software (Bioluminate, Schrödinger, LLC, New York, NY, 2020) and scored using MM-GBSA (Molecular Mechanics using Generalized Born and Surface Area continuum) scoring method (Hou et al, 2011). The top five docked complexes for β-casein-bound HtrA2 variants were analysed for the identification of interacting surface residues using PDBSum online server (Laskowski et al, 2018).

Molecular dynamic (MD) simulation analysis of bound and unbound HtrA2 variants

Both peptide-bound and unbound forms of WWW, WWΔ, WΔΔ and ΔΔΔ were subjected to MD simulation using Desmond (Desmond, Schrödinger, LLC, New York, NY, 2020) where OPLS3e (Optimized Potentials for Liquid Simulations Version 3e) force field was used to generate topology and parameter files (Harder et al, 2016; Jorgensen et al, 1996). Each protein structure was surrounded by a cubic box of TIP3P water molecules with the nearest distance from the

protein to the box boundary being no more than 10 Å (Mark & Nilsson, 2001). The generated systems were subsequently neutralized (net charge was brought to zero) by adding adequate number of positive (Na^+) ions. Each system underwent one round of steepest- descent minimization, followed by one round of conjugated gradient for 5000 picosecond (ps) (Wardi, 1988). The systems were then equilibrated in NVT (constant number of particles, volume, and temperature) and NPT (constant number of particles, pressure, and temperature) ensembles with two sets of restrained NVT (for 24 ps and 2000 ps respectively) and one set of restrained (for 24 ps) and unrestrained (for 5000 ps) NPT each (McDonald, 1972). During equilibration, LINCS (LINear Constraint Solver) constraint algorithm was used to apply position restraining force on all the atomic bonds present in the systems (Hess et al, 1997). All the systems were then subjected to final MD simulation run for 1000 nanosecond (ns) under no-restrained NPT ensemble. For peptide-bound systems, the final production runs were performed at 300 K. However, for analyzing the temperature dependent changes in the unbound systems, the final temperature was kept at 323 K. Post-simulation these systems were further subjected to meta-dynamics analysis for 50 ns that generated free energy landscape data on the basis of the active-site conformation. All the MD simulation data analysis was carried using MD simulation analysis tools available in Desmond and Maestro platform (Desmond and Maestro, Schrödinger, LLC, New York, NY, 2020).

Protein crystallization

To eliminate the possibility of partial protein degradation at higher concentrations required for crystallization, the inactive variant of N-SPD (ΔΔΔ-S306A) was used. The protein was purified in buffer containing 10 mM HEPES (pH 8.0), 100 mM NaCl, and 3% glycerol, in a similar way as described for active ΔΔΔ. Four commercial crystallization screens from Hampton Research

(HR2-110 and HR2-112) and Molecular Dimensions (Structure Screens MD1 -01 and MD1 -02) were used for setting crystallization trials using protein sample with concentration of 15 mg/ml. The optimization screen was set using hanging drop vapor diffusion after mixing protein (~6 mg/mL) in 1:1 ratio with mother liquor comprising 0.5 M Sodium acetate trihydrate, 2.0 M Sodium formate pH 6.0, 3% glycerol, and diffraction-quality crystals were obtained after two weeks at 16 °C.

Data collection and structure determination

Prior to diffraction data collection, the crystals were soaked in a cryo-protectant solution (mother liquor with 20% ethylene glycol) and then flash frozen in a liquid nitrogen stream at 100 K. Diffraction data were collected by the rotation method with a Rigaku MicroMax 007HF generator equipped with R-Axis IV++ detector using CuKα X-ray radiation (1.5418 Å) at the Protein Crystallography Facility, IIT Bombay, Mumbai. Diffraction data was collected with an exposure of 10 min, at a detector distance of 370 mm. The crystal was subjected to sequential steps of annealing (of 5 s each) for a total of 15 s. The diffraction images were indexed, integrated, and scaled with XDS (Kabsch, 2010). The intensities were converted to the structure factors with the programs F2MTZ and CAD of CCP4 (Winn et al, 2011). The data collection statistics are presented in Table 2. The calculated Matthew's coefficient for ΔΔΔ is 2.49 $Å^3$ Da^{-1} that indicated the presence of six molecules in the asymmetric unit. The phases were obtained by molecular replacement with the program PHASER (McCoy et al, 2007) using the coordinates of the N-terminal region and protease domain of the previously reported structure (PDB ID: ILCY). Further rounds of manual model building and electron density interpretation was performed in COOT (Emsley & Cowtan, 2004) and refinement was executed with REFMAC5 (Murshudov et al, 2011). The first few N-terminal residues in an asymmetric unit and the flexible loops of

certain regions could not be modeled due to the lack of proper electron density. The final refinement statistics and validation parameters obtained with MolProbity (Davis et al, 2004) of the refined structure are summarized in Table 2. All structure-related figures were generated with PyMOL (https://www.pymol.org/).

DATA AVAILABILITY

The newly solved crystal structure reported in this publication is available in RCSB PDB database (http://www.wwpdb.org) under accession number 7VGE (PDB DOI: https://doi.org/10.2210/pdb7VGE/pdb). All the other data are available in the main text or the supplementary materials. Additional data related to this paper may be requested from the authors.

ACKNOWLEDGEMENTS

We thank LK. Chaganti, N. Singh and A. Kalarikkal for their intellectual inputs and helpful suggestions related to experimentation. We are grateful to the XRD facility IIT Bombay for initial crystallization screening and crystallographic data collection. This work is supported by the Department of Biotechnology (DBT), Govt. of India (grant number BT/HRD/NWBA/37/01/2015) and intramural research grant received from ACTREC-TMC, India (IEC project no. 162).

AUTHOR CONTRIBUTIONS

Conceptualization: ALP and KB

Methodology: ALP, VM and PB (structure), SD (*in-silico*)

Investigation: ALP, VM and PB (structure), SD (*in-silico*)

Visualization: ALP, VM, SD

Supervision: ALP, PB, KB

Writing—original draft: ALP, SD (*in-silico*) and KB

Writing—review & editing: ALP, VM, SD, PB and KB

CONFLICT OF INTEREST

Authors declare that they have no competing interests.

REFERENCES

Bagowski CP, Bruins W, Te Velthuis AJW (2010) The nature of protein domain evolution: shaping the interaction network. *Curr Genomics* **11:** 368-376

Basu MK, Poliakov E, Rogozin IB (2009) Domain mobility in proteins: functional and evolutionary implications. *Brief Bioinform* **10:** 205-216

Bejugam PR, Kuppili RR, Singh N, Gadewal N, Chaganti LK, Sastry GM, Bose K (2013) Allosteric Regulation of Serine Protease HtrA2 through Novel Non-Canonical Substrate Binding Pocket. *PloS one* **8:** e55416

Bussi G, Laio A (2020) Using metadynamics to explore complex free-energy landscapes. *Nature Reviews Physics* **2:** 200-212

Cabrera AC, Melo E, Roth D, Topp A, Delobel F, Stucki C, Chen C-y, Jakob P, Banfai B, Dunkley T, Schilling O, Huber S, Iacone R, Petrone P (2017) HtrA1 activation is driven by an allosteric mechanism of inter-monomer communication. *Scientific reports* **7:** 14804

Chaganti LK, Kuppili RR, Bose K (2013) Intricate structural coordination and domain plasticity regulate activity of serine protease HtrA2. *FASEB journal : official publication of the Federation of American Societies for Experimental Biology* **27:** 3054-3066

Clausen T, Kaiser M, Huber R, Ehrmann M (2011) HTRA proteases: regulated proteolysis in protein quality control. *Nature Reviews Molecular Cell Biology* **12:** 152-162

Davis IW, Murray LW, Richardson JS, Richardson DC (2004) MolProbity: structure validation and all-atom contact analysis for nucleic acids and their complexes. *Nucleic Acids Research* **32:** W615-W619

Emsley P, Cowtan K (2004) Coot: model-building tools for molecular graphics. *Acta Crystallogr D Biol Crystallogr* **60:** 2126-2132

Gasteiger E, Hoogland C, Gattiker A, Duvaud Se, Wilkins MR, Appel RD, Bairoch A (2005) Protein Identification and Analysis Tools on the ExPASy Server. In *The Proteomics Protocols Handbook*, Walker JM (ed), pp 571-607. Totowa, NJ: Humana Press

Gieldon A, Zurawa-Janicka D, Jarzab M, Wenta T, Golik P, Dubin G, Lipinska B, Ciarkowski J (2016) Distinct 3D Architecture and Dynamics of the Human HtrA2(Omi) Protease and Its Mutated Variants. *PloS one* **11:** e0161526

Harder E, Damm W, Maple J, Wu C, Reboul M, Xiang JY, Wang L, Lupyan D, Dahlgren MK, Knight JL, Kaus JW, Cerutti DS, Krilov G, Jorgensen WL, Abel R, Friesner RA (2016) OPLS3: A Force Field Providing Broad Coverage of Drug-like Small Molecules and Proteins. *Journal of Chemical Theory and Computation* **12:** 281-296

Hasselblatt H, Kurzbauer R, Wilken C, Krojer T, Sawa J, Kurt J, Kirk R, Hasenbein S, Ehrmann M, Clausen T (2007) Regulation of the sigmaE stress response by DegS: how the PDZ domain keeps the protease inactive in the resting state and allows integration of different OMP-derived stress signals upon folding stress. *Genes & development* **21:** 2659-2670

Hess B, Bekker H, Berendsen HJC, Fraaije JGEM (1997) LINCS: A linear constraint solver for molecular simulations. *J Comput Chem* **18:** 1463-1472

Hou T, Wang J, Li Y, Wang W (2011) Assessing the performance of the molecular mechanics/Poisson Boltzmann surface area and molecular mechanics/generalized Born surface area methods. II. The accuracy of ranking poses generated from docking. *J Comput Chem* **32:** 866-877

Hung AY, Sheng M (2002) PDZ Domains: Structural Modules for Protein Complex Assembly*. *Journal of Biological Chemistry* **277:** 5699-5702

Jacobson MP, Pincus DL, Rapp CS, Day TJF, Honig B, Shaw DE, Friesner RA (2004) A hierarchical approach to all-atom protein loop prediction. *Proteins: Structure, Function, and Bioinformatics* **55:** 351-367

Jarzab M, Wenta T, Zurawa-Janicka D, Polit A, Gieldon AJ, Wysocka M, Glaza P, Skorko-Glonek J, Ciarkowski J, Lesner A, Lipinska B (2016) Intra- and intersubunit changes accompanying thermal activation of the HtrA2(Omi) protease homotrimer. *Biochimica et Biophysica Acta (BBA) - Proteins and Proteomics* **1864:** 283-296

Joanna S-G, Dorota Z-J, Tomasz K, Miroslaw J, Donata F, Przemyslaw G, Barbara L (2013) HtrA Protease Family as Therapeutic Targets. *Current Pharmaceutical Design* **19:** 977-1009

Jorgensen WL, Maxwell DS, Tirado-Rives J (1996) Development and Testing of the OPLS All-Atom Force Field on Conformational Energetics and Properties of Organic Liquids. *Journal of the American Chemical Society* **118:** 11225-11236

Kabsch W (2010) XDS. *Acta Crystallogr D Biol Crystallogr* **66:** 125-132

Kim E, Sheng M (2004) PDZ domain proteins of synapses. *Nature Reviews Neuroscience* **5:** 771-781

Laskowski RA, Jabłońska J, Pravda L, Vařeková RS, Thornton JM (2018) PDBsum: Structural summaries of PDB entries. *Protein Sci* **27:** 129-134

Lee H-J, Zheng JJ (2010) PDZ domains and their binding partners: structure, specificity, and modification. *Cell Communication and Signaling* **8:** 8

Li W, Srinivasula SM, Chai J, Li P, Wu J-W, Zhang Z, Alnemri ES, Shi Y (2002) Structural insights into the pro-apoptotic function of mitochondrial serine protease HtrA2/Omi. *Nature structural biology* **9:** 436-441

Liu Y, Patricelli MP, Cravatt BF (1999) Activity-based protein profiling: The serine hydrolases. *Proceedings of the National Academy of Sciences* **96:** 14694

Ma B, Tsai C-J, Haliloğlu T, Nussinov R (2011) Dynamic Allostery: Linkers Are Not Merely Flexible. *Structure* **19:** 907-917

Mark P, Nilsson L (2001) Structure and Dynamics of the TIP3P, SPC, and SPC/E Water Models at 298 K. *The Journal of Physical Chemistry A* **105:** 9954-9960

Martins LM, Turk BE, Cowling V, Borg A, Jarrell ET, Cantley LC, Downward J (2003) Binding Specificity and Regulation of the Serine Protease and PDZ Domains of HtrA2/Omi*. *Journal of Biological Chemistry* **278:** 49417-49427

Mauldin RV, Sauer RT (2013) Allosteric regulation of DegS protease subunits through a shared energy landscape. *Nature chemical biology* **9:** 90-96

McCoy AJ, Grosse-Kunstleve RW, Adams PD, Winn MD, Storoni LC, Read RJ (2007) Phaser crystallographic software. *J Appl Crystallogr* **40:** 658-674

McDonald IR (1972) NpT-ensemble Monte Carlo calculations for binary liquid mixtures. *Molecular Physics* **23:** 41-58

Merski M, Moreira C, Abreu RM, Ramos MJ, Fernandes PA, Martins LM, Pereira PJB, Macedo-Ribeiro S (2017a) Molecular motion regulates the activity of the Mitochondrial Serine Protease HtrA2. *Cell Death Dis* **8:** e3119-e3119

Merski M, Moreira C, Abreu RMV, Ramos MJ, Fernandes PA, Martins LM, Pereira PJB, Macedo-Ribeiro S (2017b) Molecular motion regulates the activity of the Mitochondrial Serine Protease HtrA2. *Cell death & disease* **8:** e3119-e3119

Motlagh HN, Wrabl JO, Li J, Hilser VJ (2014) The ensemble nature of allostery. *Nature* **508:** 331-339

Murshudov GN, Skubák P, Lebedev AA, Pannu NS, Steiner RA, Nicholls RA, Winn MD, Long F, Vagin AA (2011) REFMAC5 for the refinement of macromolecular crystal structures. *Acta Crystallogr D Biol Crystallogr* **67:** 355-367

Singh N, D'Souza A, Cholleti A, Sastry GM, Bose K (2014) Dual regulatory switch confers tighter control on HtrA2 proteolytic activity. *The FEBS journal* **281:** 2456-2470

Singh N, Kuppili RR, Bose K (2011) The structural basis of mode of activation and functional diversity: A case study with HtrA family of serine proteases. *Archives of biochemistry and biophysics* **516:** 85-96

Sohn J, Grant RA, Sauer RT (2007) Allosteric Activation of DegS, a Stress Sensor PDZ Protease. *Cell* **131:** 572-583

Sohn J, Grant RA, Sauer RT (2010) Allostery is an intrinsic property of the protease domain of DegS: implications for enzyme function and evolution. *The Journal of biological chemistry* **285:** 34039-34047

Spiess C, Beil A, Ehrmann M (1999) A Temperature-Dependent Switch from Chaperone to Protease in a Widely Conserved Heat Shock Protein. *Cell* **97:** 339-347

Suzuki Y, Imai Y, Nakayama H, Takahashi K, Takio K, Takahashi R (2001a) A Serine Protease, HtrA2, Is Released from the Mitochondria and Interacts with XIAP, Inducing Cell Death. *Molecular cell* **8:** 613-621

Suzuki Y, Nakabayashi Y, Nakata K, Reed JC, Takahashi R (2001b) X-linked Inhibitor of Apoptosis Protein (XIAP) Inhibits Caspase-3 and -7 in Distinct Modes *. *Journal of Biological Chemistry* **276:** 27058-27063

Toyama Y, Harkness RW, Lee TYT, Maynes JT, Kay LE (2021) Oligomeric assembly regulating mitochondrial HtrA2 function as examined by methyl-TROSY NMR. *Proceedings of the National Academy of Sciences* **118:** e2025022118

Traut T (2014) Enzyme Activity: Allosteric Regulation. *eLS*

Vierkotten S, Muether PS, Fauser S (2011) Overexpression of HTRA1 Leads to Ultrastructural Changes in the Elastic Layer of Bruch's Membrane via Cleavage of Extracellular Matrix Components. *PloS one* **6:** e22959

Walsh NP, Alba BM, Bose B, Gross CA, Sauer RT (2003) OMP Peptide Signals Initiate the Envelope-Stress Response by Activating DegS Protease via Relief of Inhibition Mediated by Its PDZ Domain. *Cell* **113:** 61-71

Wardi Y (1988) A stochastic steepest-descent algorithm. *Journal of Optimization Theory and Applications* **59:** 307-323

Wilken C, Kitzing K, Kurzbauer R, Ehrmann M, Clausen T (2004) Crystal Structure of the DegS Stress Sensor: How a PDZ Domain Recognizes Misfolded Protein and Activates a Protease. *Cell* **117:** 483-494

Winn MD, Ballard CC, Cowtan KD, Dodson EJ, Emsley P, Evans PR, Keegan RM, Krissinel EB, Leslie AGW, McCoy A, McNicholas SJ, Murshudov GN, Pannu NS, Potterton EA, Powell HR, Read RJ, Vagin A, Wilson KS (2011) Overview of the CCP4 suite and current developments. *Acta Crystallogr D Biol Crystallogr* **67:** 235-242

Yang Q-H, Church-Hajduk R, Ren J, Newton ML, Du C (2003) Omi/HtrA2 catalytic cleavage of inhibitor of apoptosis (IAP) irreversibly inactivates IAPs and facilitates caspase activity in apoptosis. *Genes & development* **17:** 1487-1496

Zhang Y, Appleton BA, Wu P, Wiesmann C, Sidhu SS (2007) Structural and functional analysis of the ligand specificity of the HtrA2/Omi PDZ domain. *Protein science : a publication of the Protein Society* **16:** 1738-1750

Zurawa-Janicka D, Jarzab M, Polit A, Skorko-Glonek J, Lesner A, Gitlin A, Gieldon A, Ciarkowski J, Glaza P, Lubomska A, Lipinska B (2013) Temperature-induced changes of HtrA2(Omi) protease activity and structure. *Cell Stress Chaperones* **18:** 35-51

TABLES

Table 1: Steady state enzyme kinetic parameters for HtrA2 variants. The initial rates for the cleavage of FITC labeled–β casein by different HtrA2 variants were measured and fitted to the Hill form of the Michaelis–Menten equation to determine the steady-state kinetic parameters (Figs 2 and EV2). Values are the mean ± SEM and are generated from data points obtained from at least three independent experiments.

HtrA2 Variants	V_{max} (Ms^{-1}) x 10^{-10}	$K_{0.5}$ (μM)	k_{cat} (s^{-1}) x 10^{-05}	k_{cat}/K_m (M^{-1} s^{-1})	Hill constant
WWW	2.892 ± 0.0002	2.513 ± 0.2	14.46	57.534	2.357 ± 0.3
WWΔ	1.360 ± 0.0007	1.738 ± 0.4	6.81	39.154	1.231 ± 0.3
WΔΔ	0.713 ± 0.0001	1.293 ± 0.1	3.57	27.578	1.272 ± 0.1
ΔΔΔ	0.289 ± 0.0001	0.869 ± 0.1	1.44	16.607	1.367 ± 0.3
W_IΔΔ	0.569 ± 0.00008	0.931 ± 0.1	2.84	30.546	1.824 ± 0.2
W_IW_IΔ	1.219 ± 0.0003	1.771 ± 0.2	6.09	34.401	2.353 ± 0.5
W$Δ_IΔ_I$	0.157 ± 0.00004	0.423 ± 0.1	0.78	18.504	2.714 ± 0.9
WW$Δ_I$	0.412 ± 0.0002	0.877 ± 0.2	2.11	24.022	2.077 ± 0.8

Table 2: Crystallography data statistics for ΔΔΔ (PDB ID: 7VGE)

Data collection and refinement statistics	**HtrA2 ΔΔΔ**
Data collection statistics	
Space group	$P4_32_12$
Unit cell parameters *a*, *b*, *c* (Å) *α*, *β*, *γ* (˚)	 82.88, 82.88, 395.31 90.00, 90.00, 90.00
Temperature (K)	100
Wavelength (Å)	1.5419
Resolution (Å)	40.0-4.0 (4.1-4.0)
R_{merge} (%)	39.8 (144.8)
Completeness (%)	90.7 (90.9)
Mean *I/σ(I)*	4.36 (1.27)
Total reflections	85456 (5452)
Unique reflections	20149 (1441)
Redundancy	4.24 (3.78)
$CC_{1/2}$	96.7 (25.1)
Wilson B factor ($Å^2$)	76.05
No. of molecules in ASU	6
Refinement statistics	
Resolution (Å)	39.53-4.0
Working set: no. of reflections	11300
R_{factor} (%)	26.51
Test set: no. of reflections	595
R_{free} (%)	33.64
Protein atoms	8149
Isotropic average B-factor (Å)	
Protein	116.3
Geometry statistics	
R.m.s.d. bond length (Å)	0.006
R.m.s.d. bond angle (°)	1.5
Ramachandran plot (%)	
Most favoured region	93.0
Allowed regions	6.7
Outlier	0.3

FIGURE LEGENDS

Figure 1: HtrA2 variants with one or two PDZ domains. (A) Schematic model depicting the denaturation-renaturation strategy that is used to generate heterotrimeric HtrA2 variants (WWΔ and WΔΔ). **(B)** Native PAGE showing generation of precisely four combinations of HtrA2 variants. Due to significant differences in pI, the electrophoretic separation of the four HtrA2 variant combinations in the renatured reaction mixture (RM) was observed in comparison to the parent homotrimers- wild type (WWW) and PDZ-deleted construct (ΔΔΔ). The concentration of the homotrimers used in this analysis was same as that used in the denaturation process to check the presence of any higher order oligomer formation at this concentration. **(C)** Western Blot analysis confirming the identity of heterotrimers. Native PAGE, as described in (B), was used for transfer of the proteins and subsequent blotting analysis. As the parent ΔΔΔ construct consisted of an N-terminal FLAG tag, the trimers containing Δ subunit (WΔΔ, WWΔ and ΔΔΔ) were easily probed in the reaction mixture using Anti-FLAG antibody. No band was probed in the WWW lane, while presence of few non-specific bands was observed in ΔΔΔ. The renatured reaction mixture was loaded in diluted form (RM^D) and in the original concentration (RM^O) to confirm the identity of heterotrimers. **(D)** SDS-PAGE showing the separation of heterotrimeric HtrA2 variants. The variants were separated from the reaction mixture using a very narrow gradient of imidazole in the elution buffer. The separation occurred on the basis of number of histidine residues present in the C-terminal His tag. WΔΔ eluted in the initial gradients, followed by WWΔ and WWW. M: Protein marker. **(E)** Native PAGE showing the separation of heterotrimeric HtrA2 variants. The separated heterotrimeric variants (WΔΔ and WWΔ indicated with filled black triangles in their respective lanes) were identified on the basis of their

electrophoretic mobility with respect to their relative position in the reaction mixture (RM^D and RM^O).

Figure 2: Time-course proteolytic cleavage assays of HtrA2 variants. (A) Qualitative gel-based proteolytic cleavage of β-casein by HtrA2 variants. 2 μg of each enzyme variant was incubated individually with 6 μg of substrate β-casein at 37 °C for different time-points between 0-90 min. The reaction at each time point was stopped with Laemmli buffer at 100 °C. Reaction samples were resolved by 12% SDS-PAGE and the cleavage pattern was visualized with Coomassie brilliant blue staining. M: Protein marker; EC: Enzyme control; SC: Substrate control. Arrows indicate the cleaved products. **(B)** Semi quantitative analysis of HtrA2 protease assays. Percentage substrate cleaved at the end of each reaction time point was calculated by quantifying the intensity of residual β-casein at each time point relative to the uncleaved substrate control (SC) using *GelQuant.NET* software and was plotted using Graphpad Prism software. WWW displayed maximum substrate cleavage activity within 5 min, followed by WWΔ and WΔΔ that cleaved 90% substrate by 5 and 10 min respectively. ΔΔΔ displayed 100% substrate cleavage between 30-60 min. The error bars represent the standard errors (SE) calculated from three independent experiments. **(C)** Quantitative assessment of the HtrA2 proteolytic activity. Initial velocities V_0 of HtrA2 and its variants were calculated using FITC labeled–β casein as the substrate. The solid lines are the nonlinear least squares fit of the data to the Hill form of the Michaelis–Menten equation: Velocity = $V_{max}/[1 + (K_{0.5}/[substrate])^n]$ using Graphpad Prism software.

Figure 3: Free energy landscape diagrams of HtrA2 variants generated on the basis of catalytic triad orientation. Contour plots for β-casein bound and temperature-induced **(A, B)** WWW, **(C, D)** WWΔ **(E, F)** WΔΔ and **(G, H)** ΔΔΔ, respectively, where each contour joined all

the structures with equal free energies (in kcal/mol). Free energies for all the variants were calculated using the intermolecular distances among the catalytic residues (H198, D228 and S306) as collective variables. The energy gradients have been represented by blue-yellow spectrum where blue represents the lowest and yellow represents the highest free energy.

Figure 4: Chemical profiling of HtrA2 variants under different activation modes. (A) Active-site modification assay performed in presence of substrate. Each variant (2 μM) was reacted with TAMRA-FP (20 μM) in absence and presence of β-casein at 37 ºC for 30 min. The reaction mixtures were run on SDS-PAGE, and fluorescence scan of the complete gel was taken using ChemiDoc™ MP Imaging System. The fluorescence intensities for the W and Δ subunits in each variant were quantified using the Image Lab™ software (version 6.0.0 build 25). The values obtained for each subunit from multiple independent experiments were averaged and the fold changes between the tests with respect to their corresponding controls were plotted using Graphpad Prism software. **(B)** Active-site modification assay performed at increased temperature. Each variant (2 μM) was reacted with TAMRA-FP (20 μM) and incubated either at 37 ºC (Control) or at 50 ºC (Test) for 30 min. The fluorescence imaging analysis and quantification were done similarly as in (A).

Figure 5: Proteolytic cleavage assays of HtrA2 variants with active-site mutation. (A) Qualitative gel-based proteolytic cleavage of β-casein by HtrA2 variants containing active-site mutation in different subunits. 2 μg of each enzyme variant was incubated individually with 6 μg of substrate β-casein and incubated at 37 °C for 30 min. The reaction at each time point was stopped with Laemmli buffer at 100 °C. Reaction samples were resolved by 12% SDS-PAGE and the cleavage pattern was visualized with Coomassie brilliant blue staining. Arrows indicate the cleaved products. M: Protein marker. **(B)** Quantitative assessment of the HtrA2 proteolytic

activity. Initial velocities V_0 of HtrA2 and its variants were calculated using FITC labeled–β casein as the substrate. The solid lines are the nonlinear least squares fit of the data to the Hill form of the Michaelis–Menten equation: Velocity = $V_{max}/[1 + (K_{0.5}/[substrate])^n]$ using Graphpad Prism software. **(C)** Model representing the *trans*-mediated allosteric communication between the adjacent subunits of HtrA2 trimeric ensemble.

Figure 6: Structural features of inactive HtrA2 ΔΔΔ variant (PDB ID: 7VGE). (A) Surface representation of the two ΔΔΔ trimers (ABC and DEF) obtained in the asymmetric unit. Left panel: Top-view of the association, with the N-terminus of one trimer (DEF) pointing outwards. Right panel: Side-view of the association, with the two trimers having their respective N-terminus pointing in opposite directions. Chains A, B, C, D, E and F are represented in pale green, pale blue, pink, pale yellow, mauve and grey respectively. **(B)** Cross-section view showing the arrangement of LA loop and the corresponding β1-β2 between two alternate chains. In the absence of C-terminal PDZ domain, a single trimer (ABC) appears to stabilize itself by associating with another similar trimer (DEF) via the LA loop. **(C)** Superposition of full-length HtrA2 (PDB ID: 1LCY – light blue) with ΔΔΔ (pale yellow). Left panel: Orientation of LA loop of 1LCY (salmon) and ΔΔΔ (Chain D) shows the absence of secondary structure for β1-β2 in ΔΔΔ. Middle panel: β7-β8 followed by LD loop (orange in 1LCY) forms an extended secondary structure in ΔΔΔ. Right panel: Absence of α5 helix (green cyan) of the PDZ domain might result in a partial loss of secondary structure of β11-β12, and absence of L2 loop (deep olive in 1LCY) in ΔΔΔ variant. **(D)** Superposition of $DegS^{\Delta PDZ}$ (PDB ID: 3LGI – green cyan) with ΔΔΔ (Chain D – pale yellow; Chain A – pale green). Conformational changes in 3LGI and ΔΔΔ are depicted in orange and green, respectively. Left panel: The LD loop shows minor conformational changes, while the L3 loop is completely missing in ΔΔΔ (chain D). Middle panel: The LA loop displays

significant difference in its orientation in 3LGI and ΔΔΔ (chain D). Right panel: Differences in orientation of L2 loop in 3LGI and ΔΔΔ (chain A). All the images were generated using PyMOL Version 1.3 (Schrodinger, LLC).

Figure 7: Model depicting different modes of HtrA2 activation. HtrA2 in the basal state exhibits very little activity, as the PDZs guard the entrance of the pyramidal ensemble and restrict the substrate entry (step Ia). Initial binding of the ligand at the exposed allosteric pocket of the PDZ of the original inactive state (E) induces subsequent conformational changes at the PDZ-protease domain interface (E_S') (step II). On the contrary, in case of activation via heat shock (step Ib), the exposed PDZs of the mature inactive protease experience increased thermal motion and induce favorable conformational changes around the active-sites in the adjacent subunits (E_T'). The primary binding or activation event leads to displacement of a single PDZ, which further commences the synergistic coordination and formation of new interaction networks between the PDZ and protease domains of adjacent subunits (E_S' or E_T'), subsequently increasing the affinity of other subunits towards the substrate by opening up the ensemble (step III) including the N-terminal region as well as rearranging the catalytic triad orientation (E*) for enhanced catalysis.

EXPANDED VIEW FIGURE LEGENDS

Figure EV1: Stick diagram showing the alignment of the catalytic triad residues for heterotrimeric variants (WWΔ and WΔΔ) and ΔΔΔ (N-SPD variant) with respect to the wild type (WWW). Catalytic residues are represented as H198, D228 and S306. Oxyanion hole residues are marked as -1, -2 and -3 starting from the S306 residue which is considered as 0. WWW, WWΔ, WΔΔ and ΔΔΔ are denoted by light blue, pink, green and yellow sticks, respectively.

Figure EV2: Ligplot showing the interacting residues between the β-casein peptide (GPFPIIV) and **A**) WWW, **B**) WWΔ, **C**) WΔΔ and **D**) ΔΔΔ variants of HtrA2. Hydrogen bond interactions are denoted by green dotted lines.

Figure EV3: Representative images from the in-gel fluorescence imaging performed for active-site modification assay using **(A)** Substrate-induced activation **(B)** Temperature-induced activation. **(C)** The fluorescence intensities of the control samples in (A) were quantified using the Image Lab™ software (version 6.0.0 build 25). The values obtained for each subunit from multiple independent experiments were plotted using Graphpad Prism software with their respective SEM. **(D)** The fluorescence intensities of the control samples in (B) were quantified and represented in a similar way as in (C).

Figure EV4: 2Fo-Fc electron density maps of regions comprising different loops in ΔΔΔ. The maps for **(A)** LA loop (165-181 residues, contoured at 0.8 σ) from chain D, and the loops **(B)** L2 (320-333 residues, contoured at 0.8 σ) and **(C)** LD (255-275 residues, contoured at 1.0 σ) from chain A are modeled. LA loop is represented as yellow ribbon, while L2 and LD loops are represented as deep olive ribbons. The map is displayed as blue mesh.

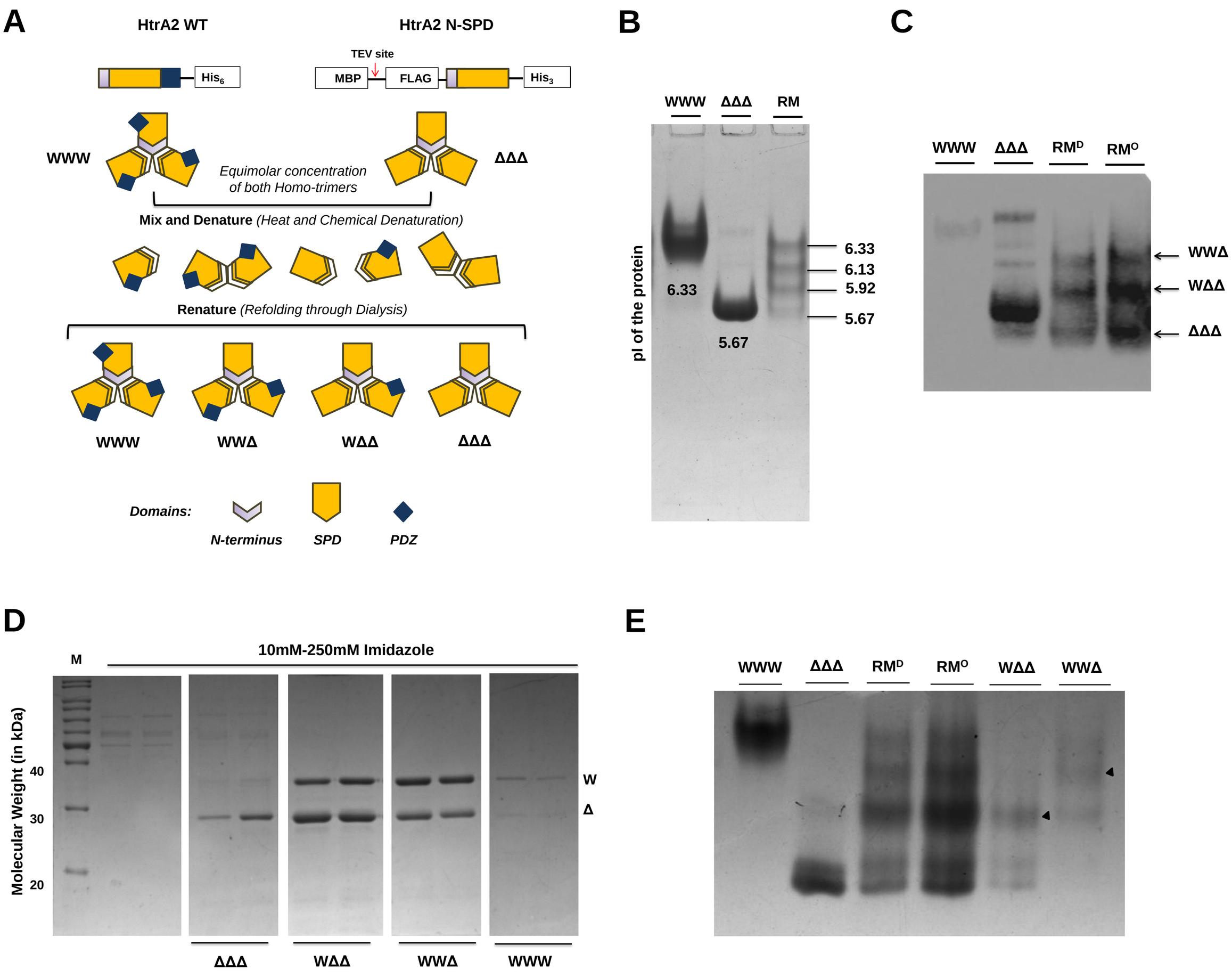
A
HtrA2 WT
HtrA2 N-SPD
TEV site
His6
MBP
FLAG
His3
WWW
ΔΔΔ
Equimolar concentration of both Homo-trimers
Mix and Denature (Heat and Chemical Denaturation)
Renature (Refolding through Dialysis)
WWW
WWΔ
WΔΔ
ΔΔΔ
Domains:
N-terminus
SPD
PDZ
B
WWW
ΔΔΔ
RM
pI of the protein
6.33
5.67
6.33
6.13
5.92
5.67
C
WWW
ΔΔΔ
RMD
RMO
WWΔ
WΔΔ
ΔΔΔ
D
M
10mM-250mM Imidazole
Molecular Weight (in kDa)
40
30
20
W
Δ
ΔΔΔ
WΔΔ
WWΔ
WWW
E
WWW
ΔΔΔ
RMD
RMO
WΔΔ
WWΔ

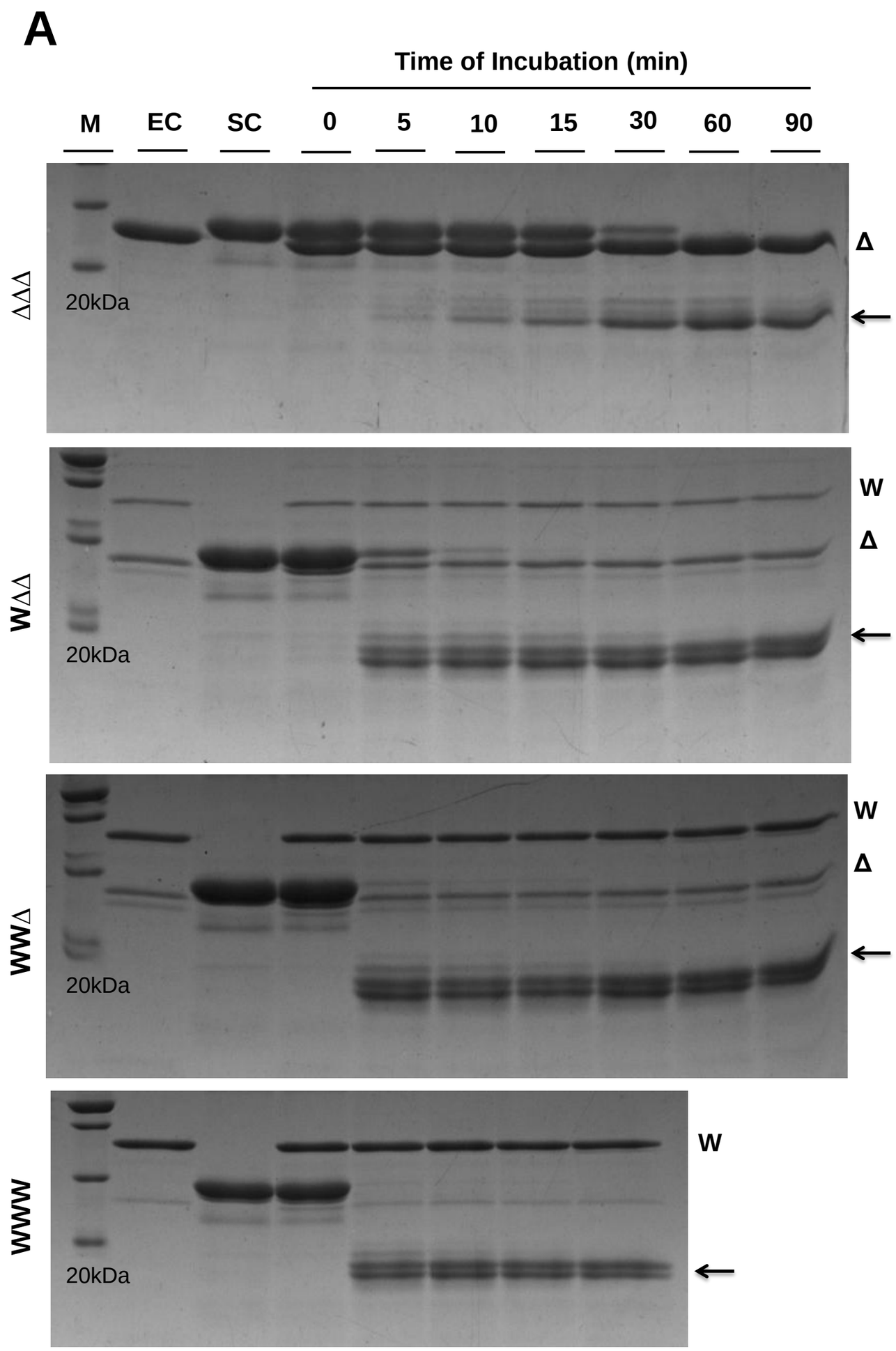
A
Time of Incubation (min)
M
EC
SC
0
5
10
15
30
60
90
ΔΔΔ
20kDa
Δ
WΔΔ
20kDa
W
Δ
WWΔ
20kDa
W
Δ
WWW
20kDa
W

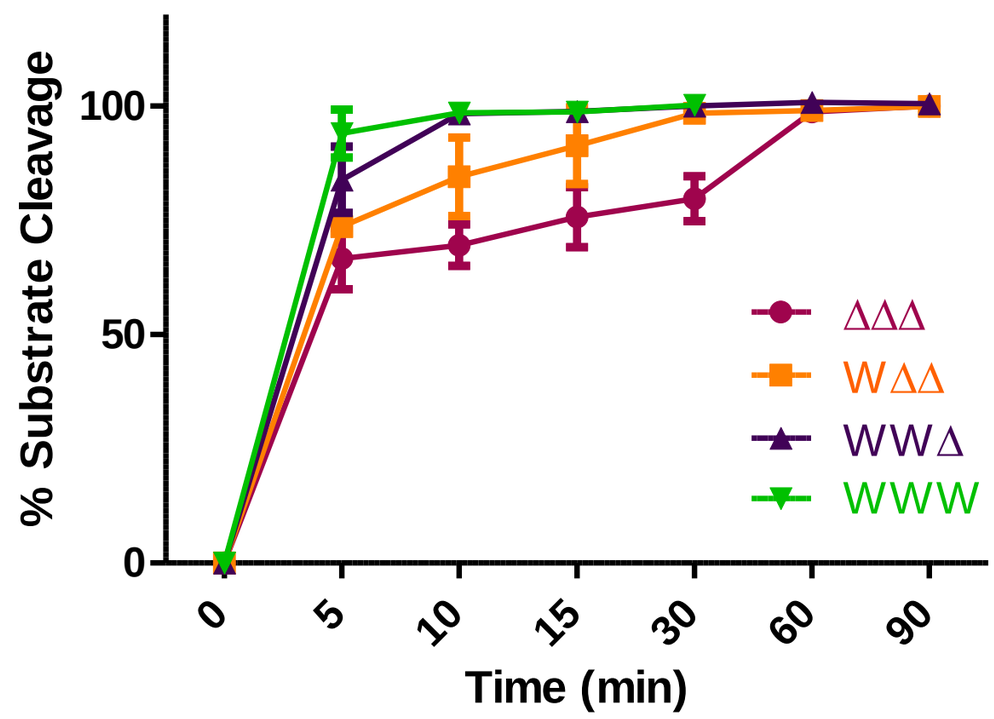
B
% Substrate Cleavage
100
50
0
0
5
10
15
30
60
90
Time (min)
ΔΔΔ
WΔΔ
WWΔ
WWW

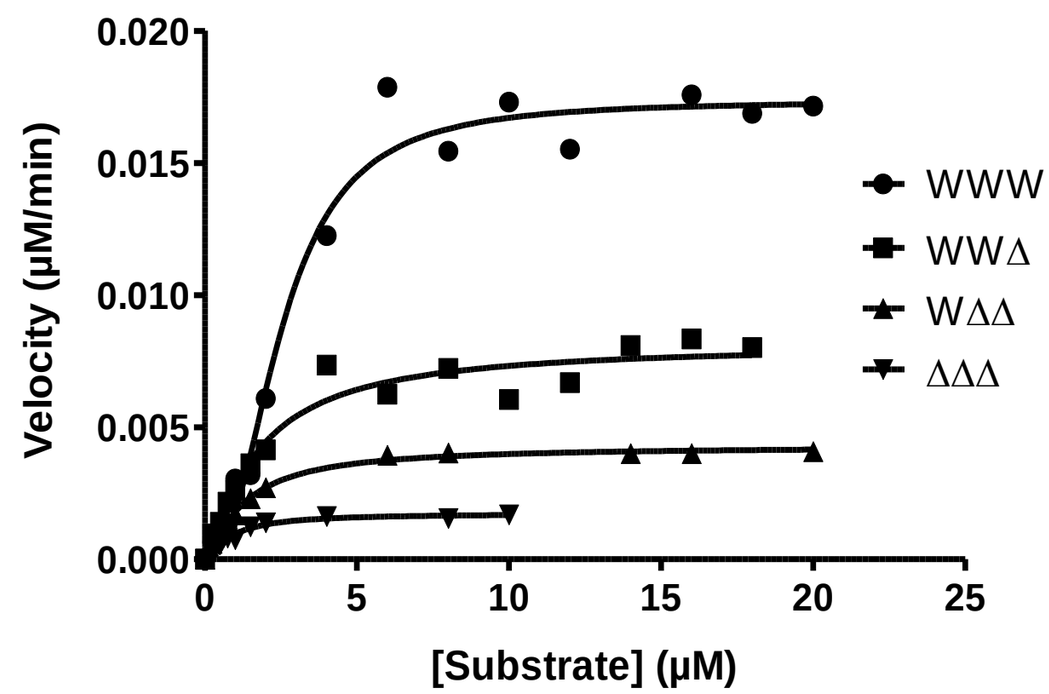
C
Velocity (μM/min)
0.020
0.015
0.010
0.005
0.000
0
5
10
15
20
25
[Substrate] (μM)
WWW
WWΔ
WΔΔ
ΔΔΔ

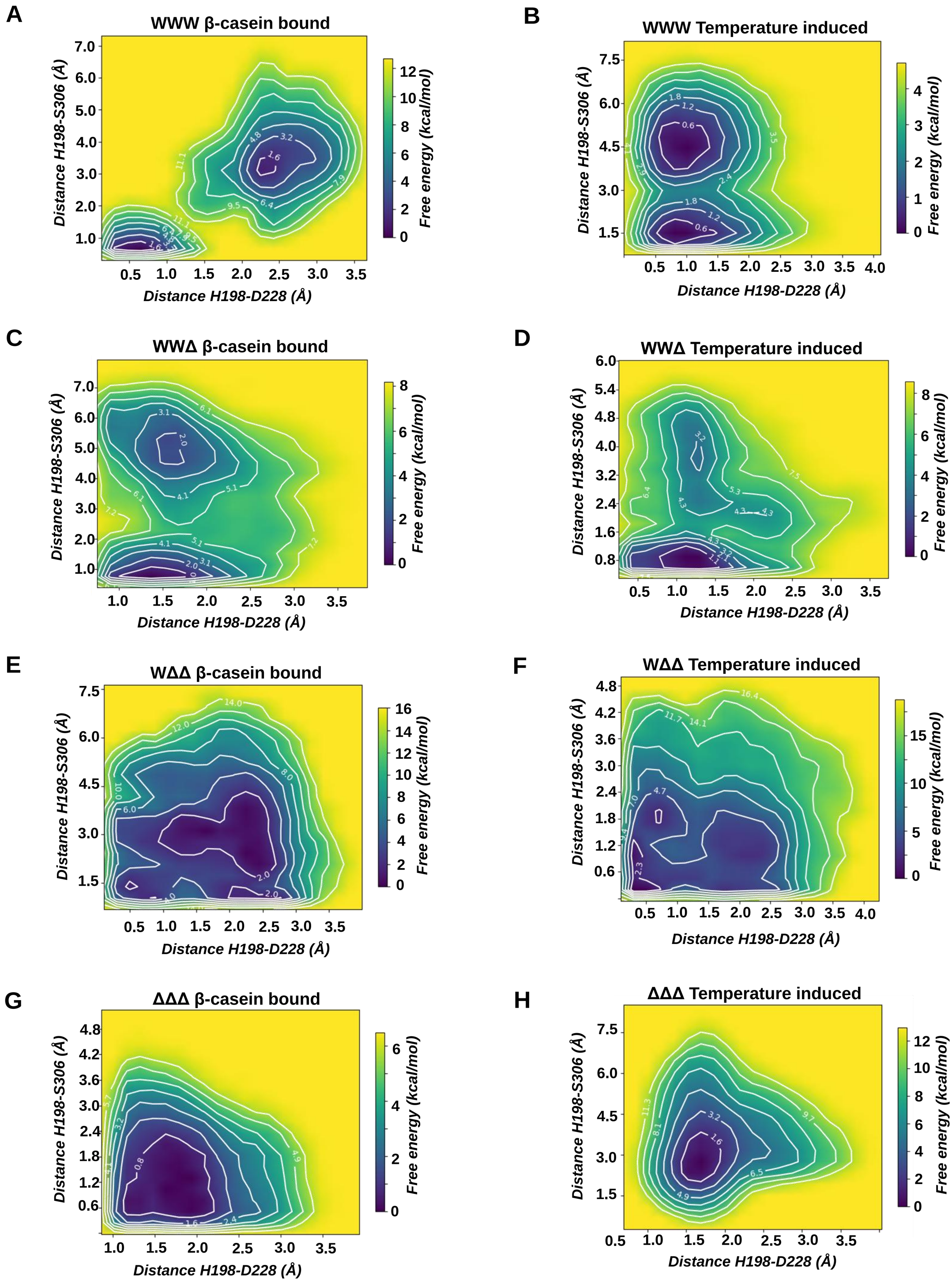
A
WWW β-casein bound
B
WWW Temperature induced
C
WWΔ β-casein bound
D
WWΔ Temperature induced
E
WΔΔ β-casein bound
F
WΔΔ Temperature induced
G
ΔΔΔ β-casein bound
H
ΔΔΔ Temperature induced
Distance H198-S306 (Å)
Distance H198-D228 (Å)
Free energy (kcal/mol)

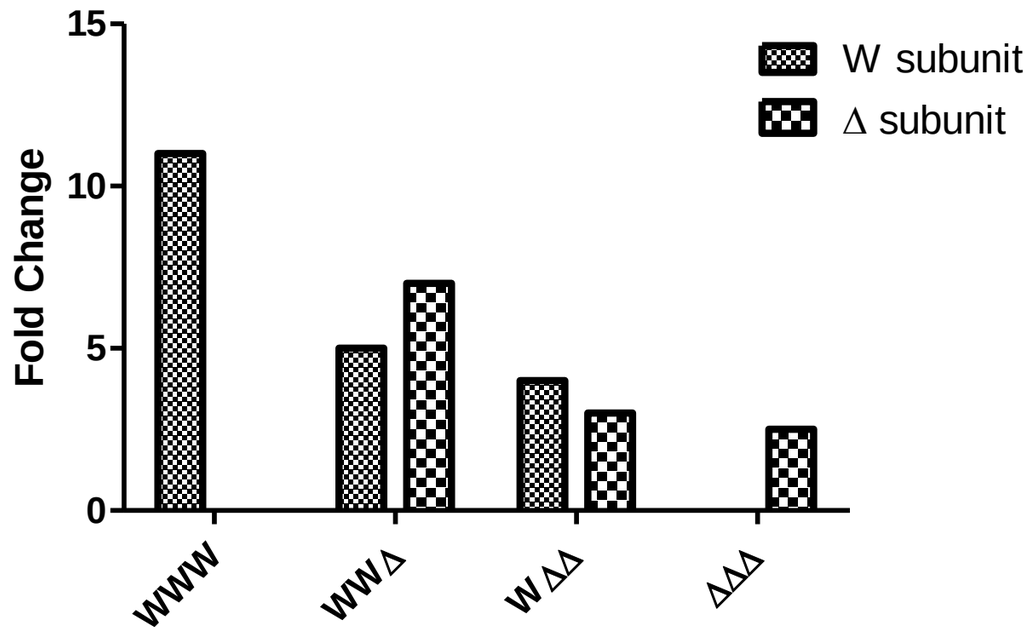
A
Substrate-induced activation
Fold Change
15
10
5
0
W subunit
Δ subunit
WWW
WWΔ
WΔΔ
ΔΔΔ

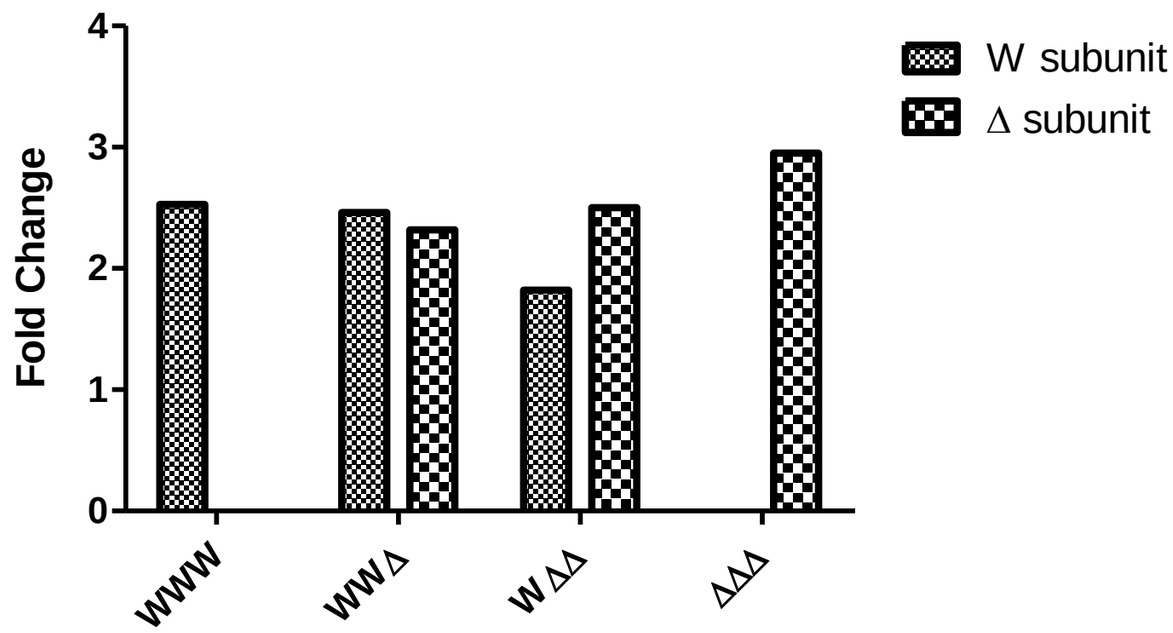
B
Temperature-induced activation
Fold Change
4
3
2
1
0
W subunit
Δ subunit
WWW
WWΔ
WΔΔ
ΔΔΔ

A

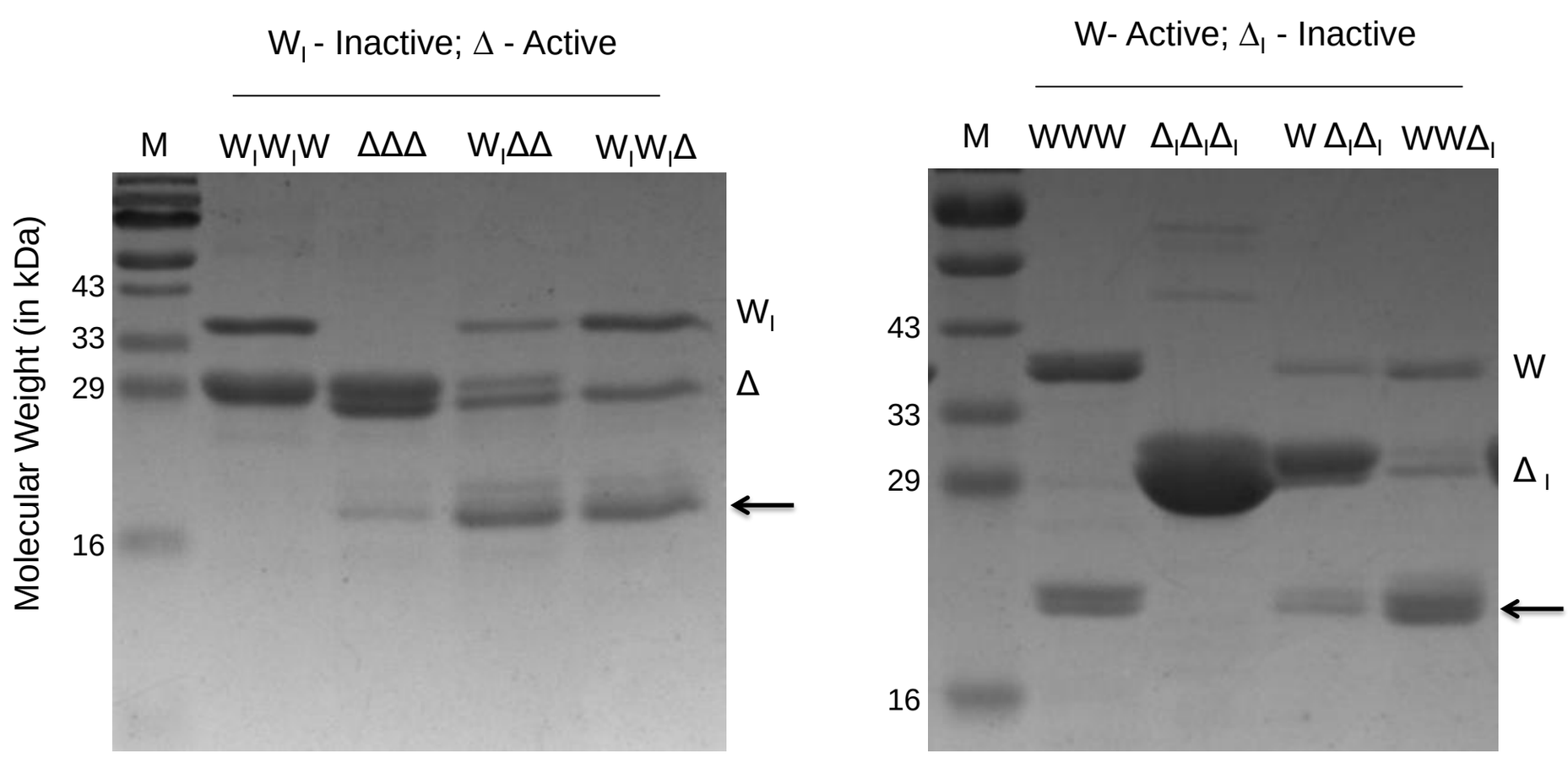

B

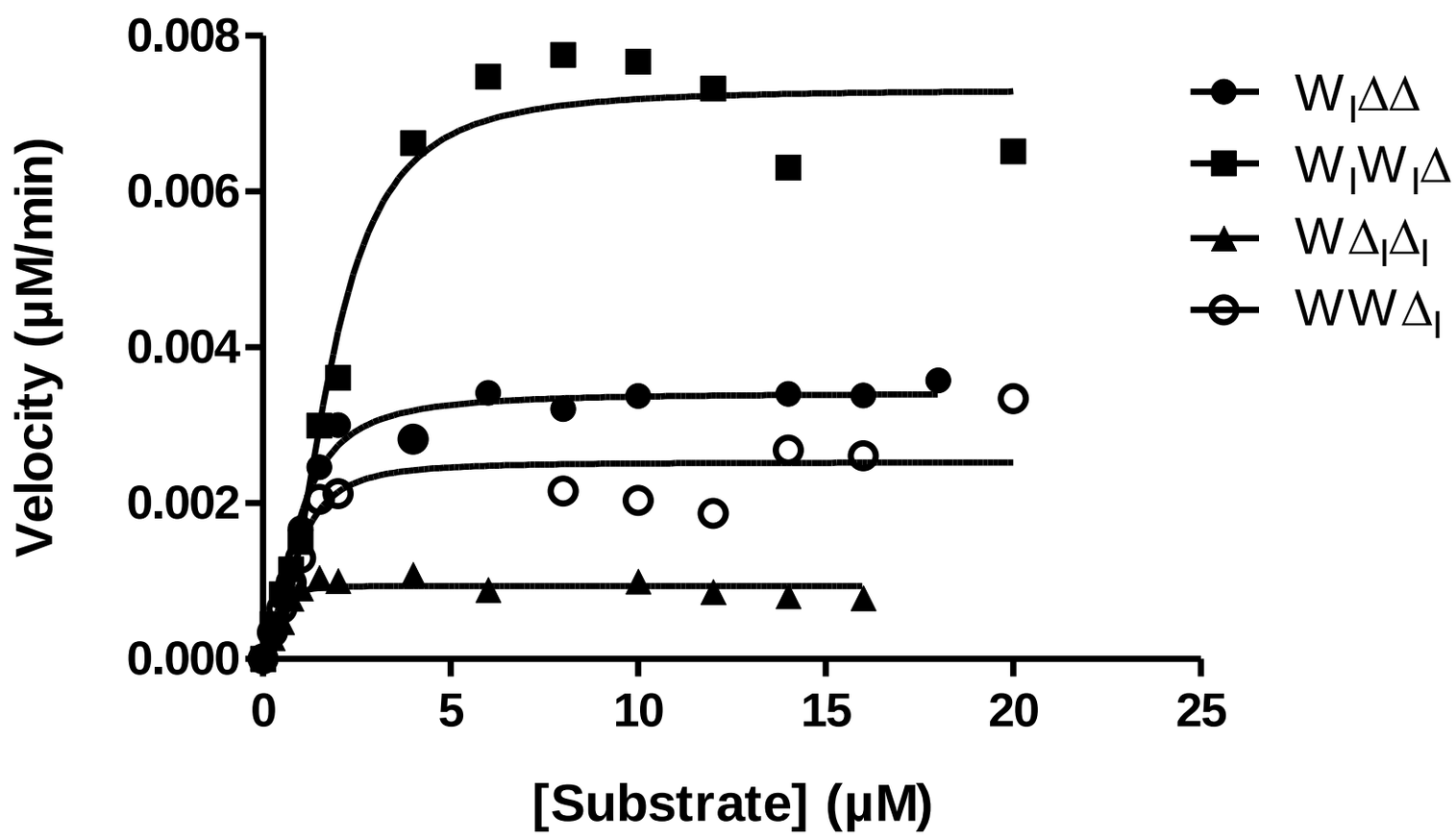

C

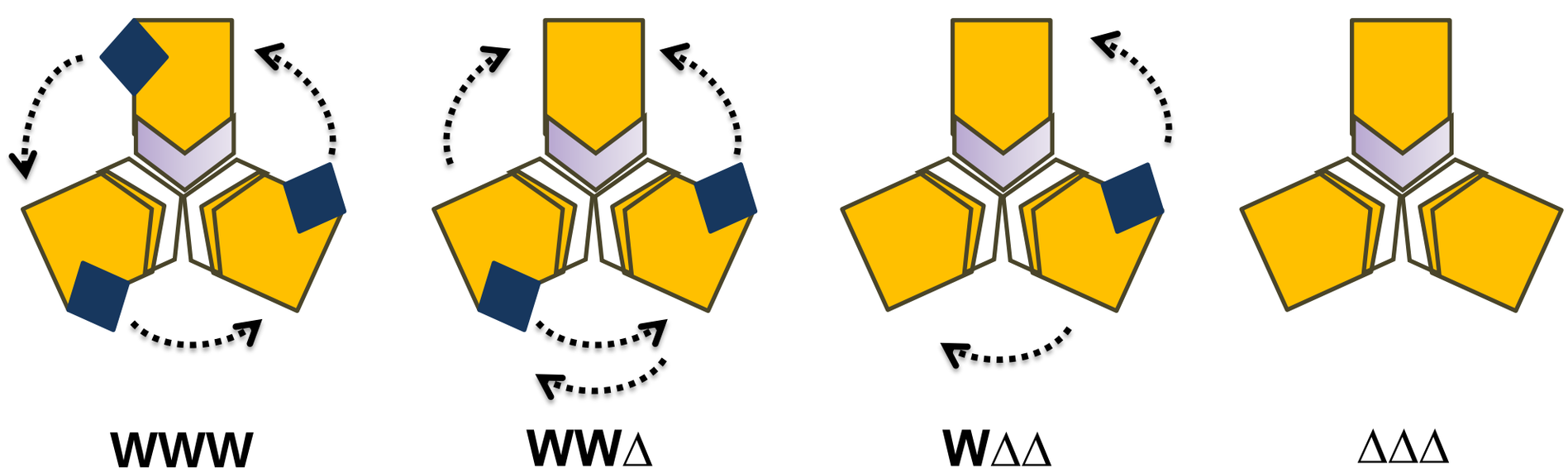

trans-mediated allosteric communication

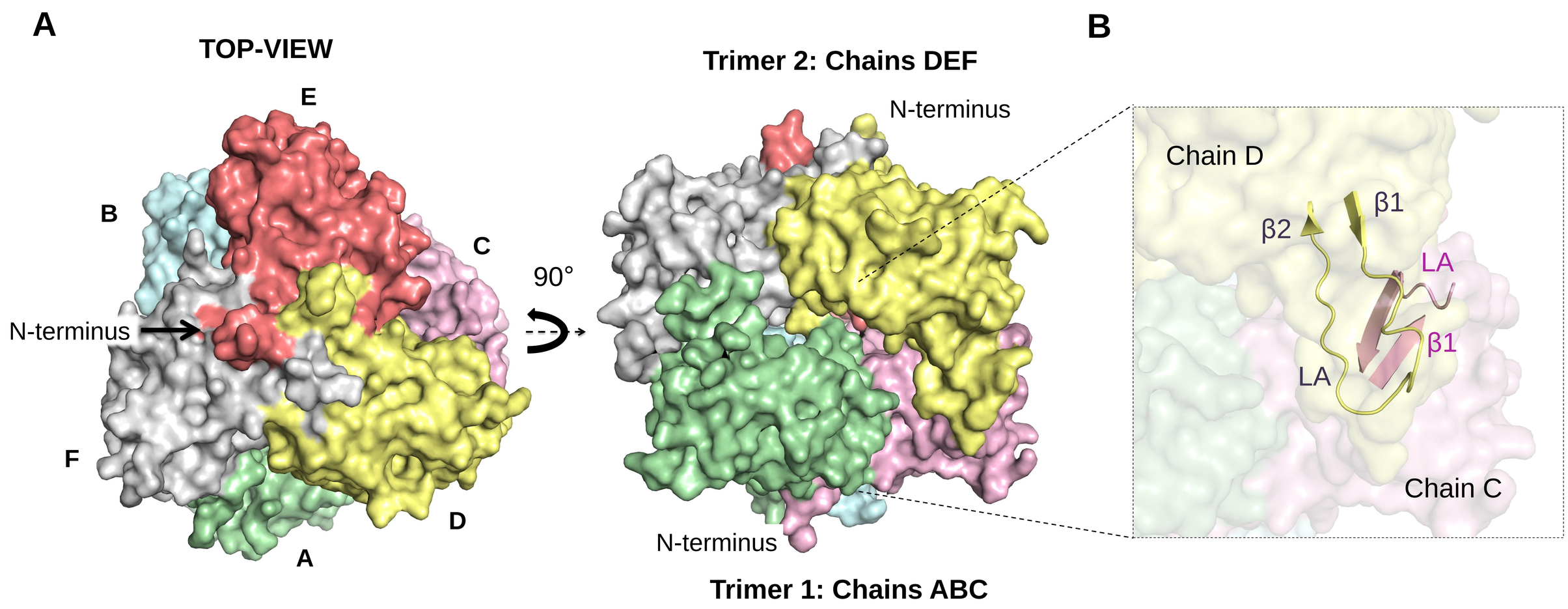
A
TOP-VIEW
E
B
C
N-terminus
F
D
A
90°
Trimer 2: Chains DEF
N-terminus
N-terminus
Trimer 1: Chains ABC
B
Chain D
β1
β2
LA
β1
LA
Chain C

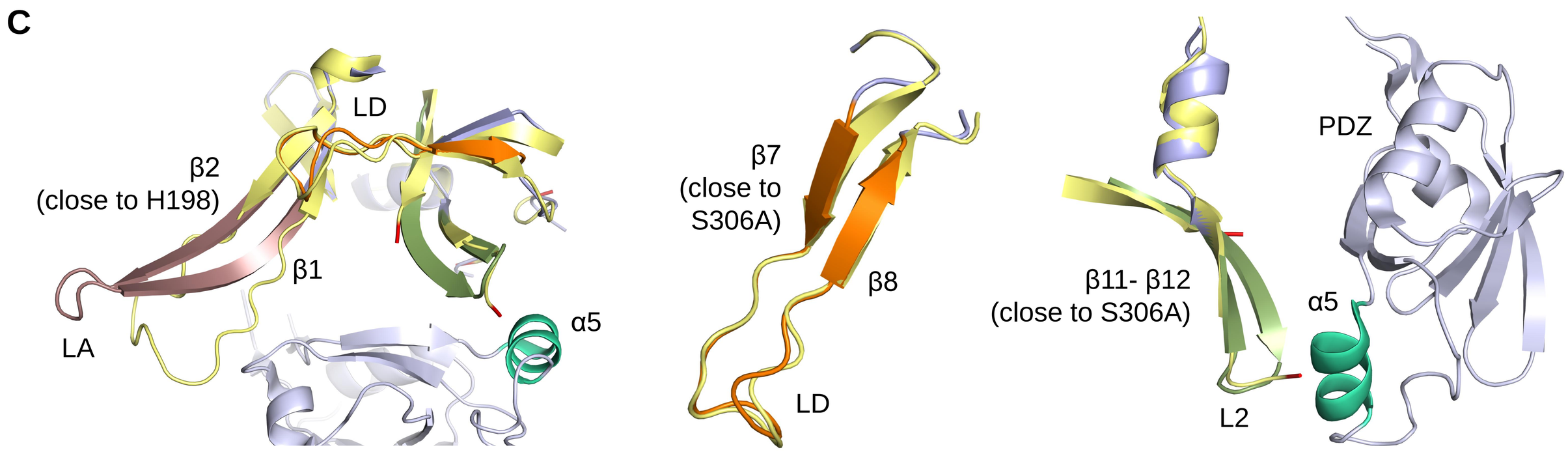
C
LD
β2
(close to H198)
β1
LA
α5
β7
(close to
S306A)
β8
LD
PDZ
β11- β12
(close to S306A)
α5
L2

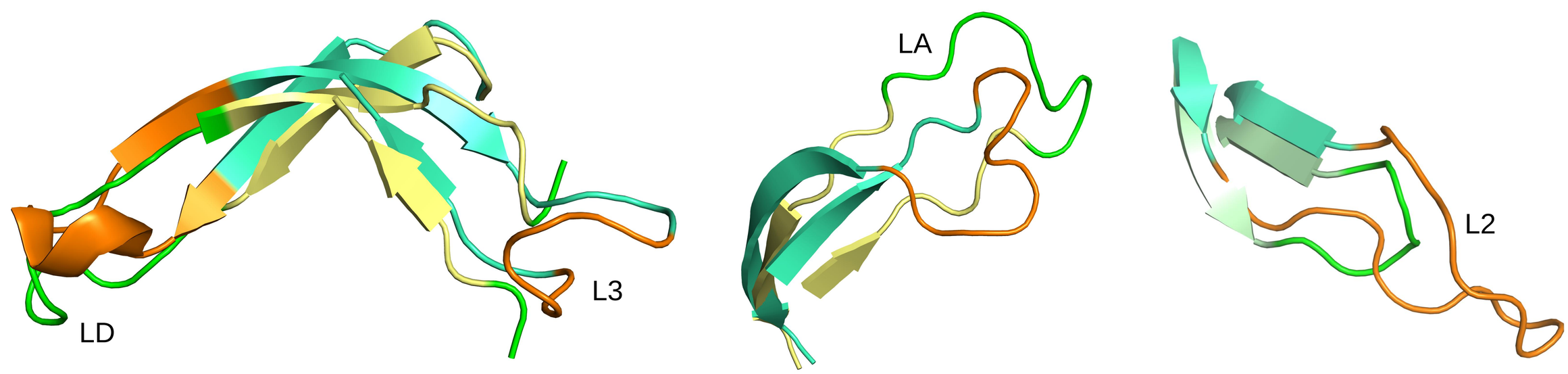
D
LD
L3
LA
L2

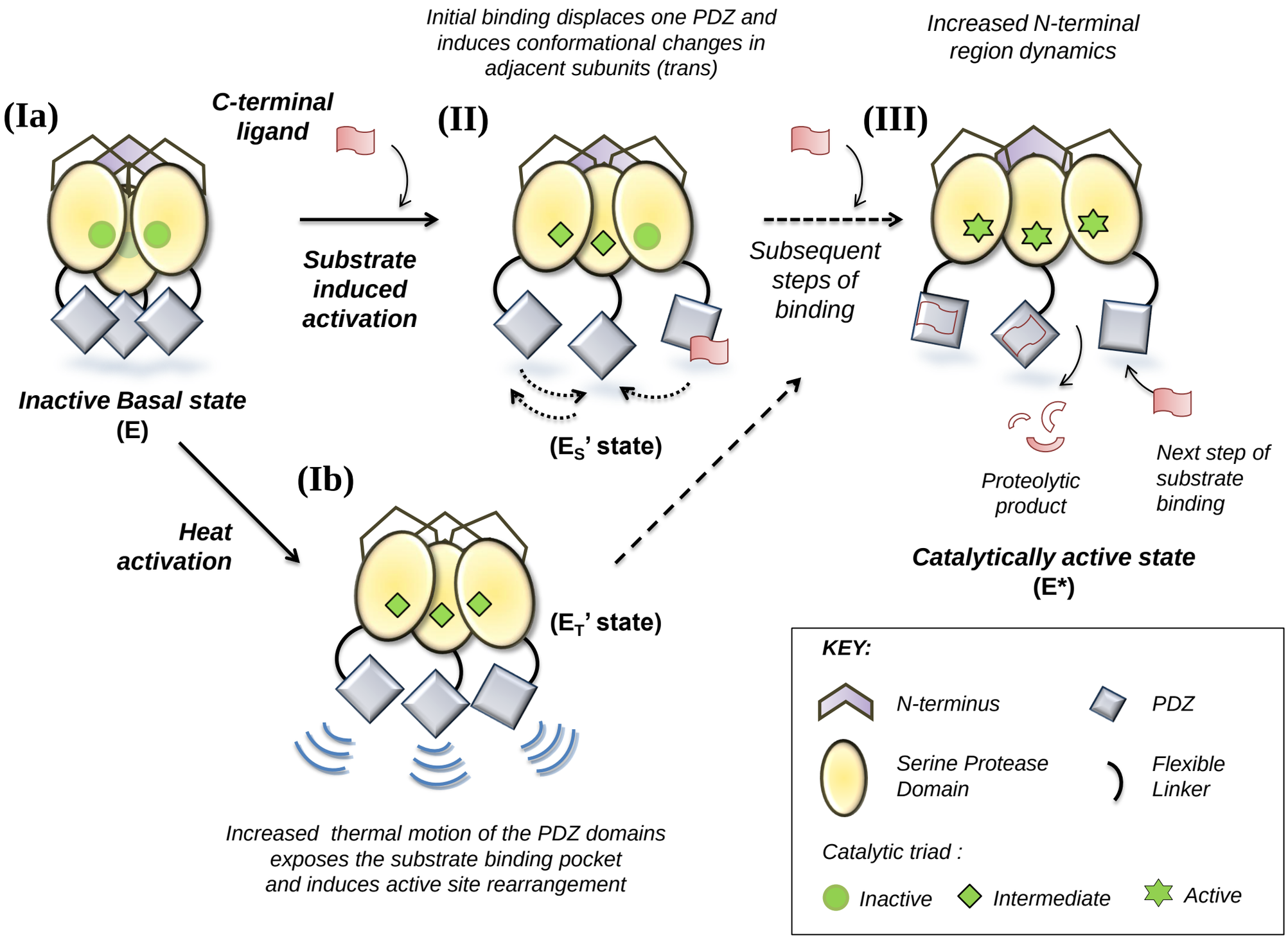
(Ia)
C-terminal ligand
Substrate induced activation
Inactive Basal state
(E)
(II)
Initial binding displaces one PDZ and induces conformational changes in adjacent subunits (trans)
(E$_S$' state)
(III)
Increased N-terminal region dynamics
Subsequent steps of binding
Proteolytic product
Next step of substrate binding
Catalytically active state
(E*)
(Ib)
Heat activation
(E$_T$' state)
Increased thermal motion of the PDZ domains exposes the substrate binding pocket and induces active site rearrangement
KEY:
N-terminus
PDZ
Serine Protease Domain
Flexible Linker
Catalytic triad :
Inactive
Intermediate
Active